

NUMERICAL ANALYSIS AND SCIENTIFIC COMPUTING
PREPRINT SERIA

**A parametrized maximum principle
preserving flux limiter for finite
difference RK-WENO schemes with
applications in incompressible flows**

T. XIONG J. QIU Z. XU

PREPRINT #19



DEPARTMENT OF MATHEMATICS
UNIVERSITY OF HOUSTON

OCTOBER 2013

A parametrized maximum principle preserving flux limiter for finite difference RK-WENO schemes with applications in incompressible flows

Tao Xiong ¹ Jing-Mei Qiu ² Zhengfu Xu ³

Abstract

In Xu [14], a class of parametrized flux limiters is developed for high order finite difference/volume essentially non-oscillatory (ENO) and Weighted ENO (WENO) schemes coupled with total variation diminishing (TVD) Runge-Kutta (RK) temporal integration for solving scalar hyperbolic conservation laws to achieve strict maximum principle preserving (MPP). In this paper, we continue along this line of research, but propose to apply the parametrized MPP flux limiter only to the final stage of any explicit RK method. Compared with the original work [14], the proposed new approach has several advantages: First, the MPP property is preserved with high order accuracy without as much time step restriction; Second, the implementation of the parametrized flux limiters is significantly simplified. Analysis is performed to justify the maintenance of third order spatial/temporal accuracy when the MPP flux limiters are applied to third order finite difference schemes solving general nonlinear problems. We further apply the limiting procedure to the simulation of the incompressible flow: the numerical fluxes of a high order scheme are limited toward that of a first order MPP scheme which was discussed in [3]. The MPP property is guaranteed, while designed high order of spatial and temporal accuracy for the incompressible flow computation is not affected via extensive numerical experiments. The efficiency and effectiveness of the proposed scheme is demonstrated via several test examples.

Keywords: hyperbolic conservation laws, high order scheme, WENO, parametrized flux limiter, maximum principle preserving, Runge-Kutta method, incompressible flow

¹Department of Mathematics, University of Houston, Houston, 77204. E-mail: txiong@math.uh.edu

²Department of Mathematics, University of Houston, Houston, 77204. E-mail: jingqiu@math.uh.edu. The first and second authors are supported by Air Force Office of Scientific Computing YIP grant FA9550-12-0318, NSF grant DMS-0914852 and DMS-1217008, University of Houston.

³Department of Mathematical Science, Michigan Technological University, Houghton, 49931. E-mail: zhengfux@mtu.edu. Supported by D90755 N49019 28399 - Start-up fund.

1 Introduction

In this paper, we consider the following scalar hyperbolic conservation laws

$$u_t + \nabla \cdot \mathbf{F}(u) = 0, \quad u(\mathbf{x}, 0) = u_0(\mathbf{x}). \quad (1.1)$$

Popular methods for solving (1.1) include finite difference/volume schemes based on high order essentially non-oscillatory (ENO) and Weighted ENO (WENO) reconstructions [2, 6] and finite element discontinuous Galerkin (DG) methods coupled with total variation diminishing (TVD) Runge-Kutta (RK) time discretization [8]. Our focus of this paper is the finite difference RK-WENO scheme. The close relationship between the finite difference and finite volume scheme was first explained by Shu and Osher [8, 9], by introducing a sliding average function $h(x)$. Compared with finite volume schemes, high order finite difference schemes are more computationally efficient for high dimensional implementations. Compared with DG, finite difference schemes with WENO reconstruction are more robust in capturing shocks without oscillations, although the finite difference schemes are not as compact and flexible in domains with complicated geometry.

An important property of the solution for hyperbolic conservation laws (1.1) is the strict maximum principle [4], namely $u_m \leq u(\mathbf{x}, t) \leq u_M$, if $u_m \leq u_0(\mathbf{x}) \leq u_M$. The TVD schemes satisfy the strict maximum principle, but it is only first order at the smooth extrema. ENO and WENO schemes are essentially non-oscillatory around discontinuities; however, the numerical solutions do not necessarily preserve the strict maximum principle. A genuinely high order conservative scheme to preserve the global maximum principle has recently been developed by Zhang and Shu in [16, 18]. MPP limiters are applied to the reconstructed high order polynomials in the finite volume/DG framework around the cell averages in order for the updated cell-average values of the numerical solutions to satisfy the maximum principle. The maintenance of high order spatial accuracy and maximum principle is theoretically proved and numerically verified when suitable CFL numbers are chosen. The techniques have recently been applied to a number of problems including the compressible/incompressible Euler equations, shallow water equations, among many others [17, 20, 13, 12]. However, it was also pointed out in [19] that it is not trivial to apply the MPP limiters to the finite difference schemes without destroying the designed order of accuracy. Also the time step size required to preserve the MPP property is smaller than the one for the original scheme, e.g. it is about $\frac{1}{6}$ of the original CFL for a third order finite volume scheme with MPP limiters [16].

In [14], Xu developed a parametrized MPP flux limiting technique to maintain the MPP property of numerical solutions of the one-dimensional scalar hyperbolic conservation laws. Compared with limiting the cell-wise reconstructed polynomials in [16, 18], in [14] the MPP property is achieved via limiting high order numerical fluxes toward first order monotone fluxes in a conservative scheme. Compared with traditional flux limiters for the TVD property (which is a stronger stability requirement than MPP), as discussed in [10, 11] and the references therein, the MPP flux limiting approach in [14] has the potential to be designed with higher than second order accuracy. The MPP requirement of $u_m \leq u_h \leq u_M$ is described by a group of explicit inequalities. By decoupling these inequalities, the numerical fluxes are locally redefined, leading to a consistent, conservative maximum principle preserving high order scheme. When coupled with the TVD RK scheme, a successive parametrized limiting approach with some ‘relaxed’ upper and lower bound is proposed for each stage of the RK method. The method was later generalized to the high order methods for solving multi-dimensional scalar hyperbolic conservation laws [15]. The MPP property is guaranteed under the same CFL time step restriction of the first order monotone scheme. However, the scheme suffers from additional time step restriction for the preservation of high order accuracy.

In this paper, following the idea in [14], we focus on developing the MPP flux limiter for conservative high order schemes, exemplified by the finite difference WENO scheme coupled with TVD RK time discretization. There are two new ingredients in this paper. First, we propose to implement the parametrized MPP flux limiters only at the final stage of the multi-stage RK time discretization. It was commented in [14] that if the MPP flux limiter is applied at each of the intermediate stage of RK method, due to the influence of the special cancellation of RK, high order temporal accuracy could be lost. With the flux limiter applied only at the final RK stage, the implementation complexity is significantly reduced. Error analysis is performed to prove the maintenance of third order spatial and temporal accuracy when the high order flux is limited toward a first order local Lax-Friedrich (LFF) flux or Godunov flux. Secondly, we apply the MPP flux limiters to the high order FD WENO method solving the incompressible Euler equation in vorticity stream-function formulation to maintain a maximum principle for vorticity. We remark that, compared with the unified high order limiting procedure for arbitrary high order reconstructed polynomials of Zhang & Shu in [16, 18], the maintenance of high order spatial and temporal accuracy so far can only be proved for the original third order finite difference scheme solving the one-dimensional nonlinear equations. We largely rely on extensive numerical experiments to

verify the maintenance of high order spatial and temporal accuracy for general high order schemes, high dimensional case, and for the incompressible flow without additional time step restriction.

The rest of the paper is organized as follows. In Section 2, we will first review the high order finite difference schemes [7] and the parametrized MPP flux limiters in Xu [14]. In Section 3, we describe on how to apply the MPP limiter on the final stage of a multi-stage RK method in one- and two-dimensional cases. Third order error analysis is provided to show that the newly proposed limiter preserves high order accuracy in both space and time without excessive time step restriction. In Section 4, MPP flux limiters are proposed for high order finite difference schemes solving incompressible flow. In Section 5, we perform numerical tests on both scalar conservation problems and incompressible Euler equations to demonstrate that maximum principle is preserved with designed order of accuracy, without additional time step restriction.

2 Review of finite difference WENO scheme [7] and parametrized MPP flux limiter [14]

2.1 Finite difference WENO scheme.

We first briefly review the finite difference WENO scheme [7] for a simple one-dimensional hyperbolic conservation equation

$$u_t + f(u)_x = 0, \quad x \in [0, 1] \quad (2.1)$$

with initial condition $u(x, 0) = u_0(x)$. Without loss of generality, we assume periodic boundary condition. We adopt the following spatial discretization for the spatial domain $[0, 1]$

$$0 = x_{\frac{1}{2}} < x_{\frac{3}{2}} < \cdots < x_{N+\frac{1}{2}} = 1,$$

where $I_j = [x_{j-\frac{1}{2}}, x_{j+\frac{1}{2}}]$ has the mesh size $\Delta x = \frac{1}{N}$. Let $u_j(t)$ denote the solution at grid point $x_j = \frac{1}{2}(x_{j-\frac{1}{2}} + x_{j+\frac{1}{2}})$ at continuous time t . The finite difference scheme evolves the point values of the solution by approximating the differential form of the equation (2.1) directly in a conservative form

$$\frac{d}{dt}u_j(t) + \frac{1}{\Delta x}(\hat{H}_{j+1/2} - \hat{H}_{j-1/2}) = 0. \quad (2.2)$$

$\hat{H}_{j+1/2} = \hat{f}(u_{j-p}, \cdots, u_{j+q})$ is a numerical flux consistent with the physical flux $f(u)$ and is Lipschitz continuous with respect to all arguments. The stencil $\{u_{j-p}, \cdots, u_{j+q}\}$ is chosen

to be upwind biased. Especially, when $f'(u) \geq 0$, one more point from the left ($p = q$) will be taken to reconstruct $\hat{f}_{j+\frac{1}{2}}$; otherwise one more point from the right ($p = q - 2$) will be taken. When $f'(u)$ changes sign over the domain, then a flux splitting, e.g. the Lax-Friedrichs flux splitting can be applied. The spatial accuracy of the scheme is determined by how well $\frac{1}{\Delta x}(\hat{H}_{j+\frac{1}{2}} - \hat{H}_{j-\frac{1}{2}})$ approximates $f(u)_x$. To obtain a high order approximation, Shu and Osher [8] introduced a sliding average function $h(x)$, such that

$$\frac{1}{\Delta x} \int_{x-\frac{\Delta x}{2}}^{x+\frac{\Delta x}{2}} h(\xi) d\xi = f(u(x, t)). \quad (2.3)$$

Taking the x derivative of the above equation gives

$$\frac{1}{\Delta x} \left(h\left(x + \frac{\Delta x}{2}\right) - h\left(x - \frac{\Delta x}{2}\right) \right) = f(u)_x. \quad (2.4)$$

Therefore the numerical flux $\hat{H}_{j+\frac{1}{2}}$ in equation (2.2) can be taken as $h(x_{j+\frac{1}{2}})$, which can be reconstructed from neighboring cell averages of $h(x)$, $\bar{h}_i = \frac{1}{\Delta x} \int_{I_i} h(\xi) d\xi \stackrel{(2.3)}{=} f(u(x_i, t))$, $i = j - p, \dots, j + q$ by WENO reconstruction. By adaptively assigning nonlinear weights to neighboring candidate stencils, the WENO reconstruction preserves high order accuracy of the linear scheme around smooth regions of the solution, while producing a sharp and essentially non-oscillatory capture of discontinuities. Equation (2.2) can be further discretized in time by a high order time integrator. For example, the scheme with the first order forward Euler time discretization is

$$u_j^{n+1} = u_j^n - \lambda(\hat{H}_{j+1/2} - \hat{H}_{j-1/2}), \quad (2.5)$$

where u_j^n denotes the numerical solution at x_j and at time t^n , $\lambda = \frac{\Delta t}{\Delta x}$ and Δt is the time step size.

The finite difference WENO schemes have been extended to the adaptive mesh refinement (AMR) framework [5] and have been applied to a wide range of problems including computational fluid dynamics, astrophysics, plasma physics, semi-conductor device simulations among many others [7]. It is well-known that the schemes enjoy the mass conservation, high order spatial accuracy, and the flexibility in implementation for high dimensional problems when compared with the finite volume framework. However, the maximum principle preserving (MPP) property of the solution for hyperbolic equation (2.1) is not preserved on the numerical level. For more details, please see [7] and the references therein.

2.2 A parametrized MPP flux limiter [14]

Below, we illustrate the idea of parametrized flux limiters for preserving the maximum principle of the high order finite difference scheme. For simplicity, we first consider the one step forward Euler time discretization. The idea will be generalized to a high order TVD Runge-Kutta time discretization in the next section.

Let

$$u_m = \min_x(u(x, 0)), \quad u_M = \max_x(u(x, 0)).$$

To preserve the MPP property

$$u_m \leq u_j^n \leq u_M, \quad \forall j, n \quad (2.6)$$

it is proposed in [14] to modify the numerical fluxes $\hat{H}_{j+1/2}$ as

$$\tilde{H}_{j+1/2} = \theta_{j+1/2}(\hat{H}_{j+1/2} - \hat{h}_{j+1/2}) + \hat{h}_{j+1/2} \quad (2.7)$$

where $\hat{h}_{j+1/2} = \hat{f}(u_j, u_{j+1})$ is the first order monotone flux. Notice that with the first order monotone flux in equation (2.5), it is well-known that the MPP property (2.6) will be preserved. $\theta_{j+1/2} \in [0, 1]$ is designed by taking advantage of the MPP property with the use of the first order monotone flux $\hat{h}_{j+1/2}$ and the high order accuracy of $\hat{H}_{j+1/2}$ reconstructed from WENO procedure.

Below is a detailed procedure of designing $\theta_{j+1/2}$. For each $\theta_{j+1/2}$ limiting the numerical flux $\tilde{H}_{j+1/2}$, we are looking for upper bounds $\Lambda_{-1/2, I_j}$ and $\Lambda_{+1/2, I_j}$ from the need of keeping u_j^{n+1} within $[u_m, u_M]$. Consequently,

$$\theta_{j+1/2} \in [0, \Lambda_{+1/2, I_j}] \cap [0, \Lambda_{-1/2, I_{j+1}}], \quad \forall j \quad (2.8)$$

provides a sufficient condition for the scheme to preserve the maximum principle. Let

$$\Gamma_j^M = u_M - u_j + \lambda(\hat{h}_{j+1/2} - \hat{h}_{j-1/2}), \quad \Gamma_j^m = u_m - u_j + \lambda(\hat{h}_{j+1/2} - \hat{h}_{j-1/2}),$$

then from the MPP property of a first order monotone scheme,

$$\Gamma_j^M \geq 0, \quad \Gamma_j^m \leq 0.$$

To ensure $u_j^{n+1} \in [u_m, u_M]$ with $\tilde{H}_{j+1/2}$ as in equation (2.7), it is sufficient to have

$$\lambda\theta_{j-1/2}(\hat{H}_{j-1/2} - \hat{h}_{j-1/2}) - \lambda\theta_{j+1/2}(\hat{H}_{j+1/2} - \hat{h}_{j+1/2}) - \Gamma_j^M \leq 0, \quad (2.9)$$

$$\lambda\theta_{j-1/2}(\hat{H}_{j-1/2} - \hat{h}_{j-1/2}) - \lambda\theta_{j+1/2}(\hat{H}_{j+1/2} - \hat{h}_{j+1/2}) - \Gamma_j^m \geq 0. \quad (2.10)$$

The discussion is case by case based on the sign of

$$F_{j\pm 1/2} \doteq \hat{H}_{j\pm 1/2} - \hat{h}_{j\pm 1/2}.$$

1. Assume

$$\theta_{j-1/2} \in [0, \Lambda_{-1/2, I_j}^M], \quad \theta_{j+1/2} \in [0, \Lambda_{+1/2, I_j}^M],$$

where $\Lambda_{-1/2, I_j}^M$ and $\Lambda_{+1/2, I_j}^M$ are designed to preserve the upper bound by equation (2.9)

(a) If $F_{j-1/2} \leq 0$ and $F_{j+1/2} \geq 0$,

$$(\Lambda_{-1/2, I_j}^M, \Lambda_{+1/2, I_j}^M) = (1, 1).$$

(b) If $F_{j-1/2} \leq 0$ and $F_{j+1/2} < 0$,

$$(\Lambda_{-1/2, I_j}^M, \Lambda_{+1/2, I_j}^M) = (1, \min(1, \frac{\Gamma_j^M}{-\lambda F_{j+1/2}})).$$

(c) If $F_{j-1/2} > 0$ and $F_{j+1/2} \geq 0$,

$$(\Lambda_{-1/2, I_j}^M, \Lambda_{+1/2, I_j}^M) = (\min(1, \frac{\Gamma_j^M}{\lambda F_{j-1/2}}), 1).$$

(d) If $F_{j-1/2} > 0$ and $F_{j+1/2} < 0$,

- If equation (2.9) is satisfied with $(\theta_{j-1/2}, \theta_{j+1/2}) = (1, 1)$, then

$$(\Lambda_{-1/2, I_j}^M, \Lambda_{+1/2, I_j}^M) = (1, 1).$$

- If equation (2.9) is not satisfied with $(\theta_{j-1/2}, \theta_{j+1/2}) = (1, 1)$, then

$$(\Lambda_{-1/2, I_j}^M, \Lambda_{+1/2, I_j}^M) = (\frac{\Gamma_j^M}{\lambda F_{j-1/2} - \lambda F_{j+1/2}}, \frac{\Gamma_j^M}{\lambda F_{j-1/2} - \lambda F_{j+1/2}}).$$

2. Similarly assume

$$\theta_{j-1/2} \in [0, \Lambda_{-1/2, I_j}^m], \quad \theta_{j+1/2} \in [0, \Lambda_{+1/2, I_j}^m],$$

where $\Lambda_{-1/2, I_j}^m$ and $\Lambda_{+1/2, I_j}^m$ are designed to preserve the lower bound by equation (2.10).

(a) If $F_{j-1/2} \geq 0$ and $F_{j+1/2} \leq 0$,

$$(\Lambda_{-1/2, I_j}^m, \Lambda_{+1/2, I_j}^m) = (1, 1).$$

(b) If $F_{j-1/2} \geq 0$ and $F_{j+1/2} > 0$,

$$(\Lambda_{-1/2, I_j}^m, \Lambda_{+1/2, I_j}^m) = (1, \min(1, \frac{\Gamma_j^m}{-\lambda F_{j+1/2}})).$$

(c) If $F_{j-1/2} < 0$ and $F_{j+1/2} \leq 0$,

$$(\Lambda_{-1/2, I_j}^m, \Lambda_{+1/2, I_j}^m) = (\min(1, \frac{\Gamma_j^m}{\lambda F_{j-1/2}}), 1).$$

(d) If $F_{j-1/2} < 0$ and $F_{j+1/2} > 0$,

- If equation (2.10) is satisfied with $(\theta_{j-1/2}, \theta_{j+1/2}) = (1, 1)$, then

$$(\Lambda_{-1/2, I_j}^m, \Lambda_{+1/2, I_j}^m) = (1, 1).$$

- If equation (2.10) is not satisfied with $(\theta_{j-1/2}, \theta_{j+1/2}) = (1, 1)$, then

$$(\Lambda_{-1/2, I_j}^m, \Lambda_{+1/2, I_j}^m) = (\frac{\Gamma_j^m}{\lambda F_{j-1/2} - \lambda F_{j+1/2}}, \frac{\Gamma_j^m}{\lambda F_{j-1/2} - \lambda F_{j+1/2}}).$$

Notice that the range of $\theta_{j+1/2}$ (2.8) is determined by the need to ensure both the upper bound (2.9) and the lower bound (2.10) of numerical solutions in both cell I_j and I_{j+1} . Thus the locally defined limiting parameter is given as

$$\theta_{j+1/2} = \min(\Lambda_{+1/2, I_j}, \Lambda_{-1/2, I_{j+1}}), \quad (2.11)$$

with $\Lambda_{+1/2, I_j} = \min(\Lambda_{+1/2, I_j}^M, \Lambda_{+1/2, I_j}^m)$, $\Lambda_{-1/2, I_{j+1}} = \min(\Lambda_{-1/2, I_{j+1}}^M, \Lambda_{-1/2, I_{j+1}}^m)$. The modified flux in equation (2.7) with the $\theta_{j+1/2}$ designed above ensures the maximum principle. Such modified flux is consistent and monotone since it is a convex combination ($\theta_{j+1/2} \in [0, 1]$) of a high order flux $\hat{H}_{j+1/2}$ with the first order flux $\hat{h}_{j+1/2}$. Since the scheme is in the flux difference form (2.5), the mass conservation property is preserved. It is proven in [14] that if the time step size Δt is small enough, fourth order spatial accuracy of the scheme with regular WENO flux $\hat{H}_{j+1/2}$ is maintained with the modified flux $\tilde{H}_{j+1/2}$ for the linear case.

3 A new parametrized MPP limiter for the RK-WENO

3.1 One-dimensional problem

A ‘successive’ MPP limiting procedure was proposed in [14] for limiting the upper and lower bounds of solutions at internal stages of a third order TVD RK method [1]. In this

section, we propose to apply the MPP flux limiting procedure at the final stage of RK time discretization only. The newly proposed limiting procedure is very general in the sense that it can be applied to any high order explicit RK method. Moreover, the time step restriction to ensure both MPP property and high order accuracy in both space and time is relieved compared with that proposed in [14], see Theorem 3.2 below.

To illustrate the idea, without loss of generality, we use a third order TVD RK time discretization below as an example. With the method-of-lines approach, the third order TVD RK time discretization [1] can be written as

$$\begin{aligned} u^{(1)} &= u^n + \Delta t L(u^n), \\ u^{(2)} &= u^n + \Delta t \left(\frac{1}{4} L(u^n) + \frac{1}{4} L(u^{(1)}) \right), \\ u^{n+1} &= u^n + \Delta t \left(\frac{1}{6} L(u^n) + \frac{2}{3} L(u^{(2)}) + \frac{1}{6} L(u^{(1)}) \right). \end{aligned} \quad (3.1)$$

We note that the second term in equation (3.1) approximates $\int_{t^n}^{t^{n+1}} L(u(\tau)) d\tau$. Here $L(u^n) \doteq -\frac{1}{\Delta x} (\hat{H}_{j+\frac{1}{2}}^n - \hat{H}_{j-\frac{1}{2}}^n)$, where $\hat{H}_{j+\frac{1}{2}}^n$ is the numerical flux from WENO reconstruction based on u^n . Similarly, let $\hat{H}_{j+\frac{1}{2}}^{(1)}$ and $\hat{H}_{j+\frac{1}{2}}^{(2)}$ be the numerical fluxes reconstructed based on $u^{(1)}$ and $u^{(2)}$. The equation (3.1) can be rewritten as

$$u_j^{n+1} = u_j^n - \lambda (\hat{H}_{j+\frac{1}{2}}^{rk} - \hat{H}_{j-\frac{1}{2}}^{rk}), \quad (3.2)$$

where

$$\hat{H}_{j+\frac{1}{2}}^{rk} \doteq \frac{1}{6} \hat{H}_{j+\frac{1}{2}}^n + \frac{2}{3} \hat{H}_{j+\frac{1}{2}}^{(2)} + \frac{1}{6} \hat{H}_{j+\frac{1}{2}}^{(1)}.$$

Based on equation (3.2), we propose to replace the numerical flux $\hat{H}_{j+\frac{1}{2}}^{rk}$ by the modified one

$$\tilde{H}_{j+\frac{1}{2}}^{rk} = \theta_{j+\frac{1}{2}} (\hat{H}_{j+\frac{1}{2}}^{rk} - \hat{h}_{j+\frac{1}{2}}) + \hat{h}_{j+\frac{1}{2}} \quad (3.3)$$

where $\hat{h}_{j+\frac{1}{2}}$ is the first order monotone flux and $\theta_{j+\frac{1}{2}}$ is designed in the same way as that in the review Section 2.2 to preserve the MPP property. It shall be pointed out that most of the explicit RK temporal approximation method can be written in the form of (3.2). Therefore, the newly proposed MPP flux limiting procedure can be directly applied to most of the high order conservative schemes equipped with an explicit RK temporal integration. It is proven in Theorem 3.2 below that the proposed flux limiters maintain high order spatial accuracy of the original finite difference scheme and temporal accuracy of RK discretization.

Remark 3.1. The proposed flux limiting procedure is very simple and computationally efficient, compared with that in [14]. Notice that numerical solutions at intermediate RK

stages, i.e. $u^{(1)}$ and $u^{(2)}$, are low order in time approximations to the exact solutions at the corresponding stages. If the MPP properties are enforced at these intermediate stages, the special cancellation of RK method may be affected. As a result, very restrictive time step size would be needed to maintain high order accuracy in time, see [14].

In the following, we will show that the high order accuracy in both space and time is maintained with the newly proposed MPP limiter when the solution is smooth enough. As there is no rigorous error analysis for finite difference scheme with high order reconstruction by introducing the sliding function $h(x)$ and high order RK method for hyperbolic equation (2.1), we make some assumptions on the error of the original high order finite difference scheme. Notice that these assumptions have been numerically verified extensively, but haven't been rigorously proven. In the Theorem below, we rigorously justify that the amount of modification performed by the parametrized flux limiter is of high order.

Theorem 3.2. *Consider solving advection equation (2.1) using a third order finite difference spatial discretization and a third order RK time discretization with the scheme written in the form of equation (3.2). Assume the global error,*

$$e_j^n = |u_j^n - u(x_j, t^n)| = \mathcal{O}(\Delta x^3 + \Delta t^3), \quad \forall n, j. \quad (3.4)$$

Consider applying the proposed MPP limiter to the numerical fluxes $\hat{H}_{j\pm\frac{1}{2}}^{rk}$ in equation (3.2), and taking $\hat{h}_{j+\frac{1}{2}}$ in equation (3.3) to be the local Lax-Friedrichs (LLF) flux, then

$$|\hat{H}_{j+\frac{1}{2}}^{rk} - \tilde{H}_{j+\frac{1}{2}}^{rk}| = \mathcal{O}(\Delta x^3 + \Delta t^3), \quad \forall j, \quad (3.5)$$

with $\lambda \max_u |f'(u)| \leq 1$, where $\lambda = \Delta t / \Delta x$.

Proof. We only consider the limiters for the maximum value case, it is similar for the minimum value case. The statement is proved via discussing four cases described in Section 2.2. Without specifying, we use u_j instead of u_j^n and use $u(x)$ instead of $u(x, t^n)$. From our assumption (3.4), the difference between $u(x_j, t^n)$ and u_j^n is of high order. In our proof below, we use $u(x_j, t^n)$ and u_j^n interchangeably when such high order difference allows.

Case (a): No limiters are introduced in case (a) decoupling, therefore equation (3.5) holds.

Case (d): This is the case of $F_{j-\frac{1}{2}} > 0$ and $F_{j+\frac{1}{2}} < 0$. From (3.3), it is sufficient to show that

$$\frac{\Gamma_j^M - (\lambda F_{j-\frac{1}{2}} - \lambda F_{j+\frac{1}{2}})}{\lambda F_{j-\frac{1}{2}} - \lambda F_{j+\frac{1}{2}}} F_{j+\frac{1}{2}} = \mathcal{O}(\Delta x^3 + \Delta t^3), \quad (3.6)$$

when $\Gamma_j^M < \lambda F_{j-\frac{1}{2}} - \lambda F_{j+\frac{1}{2}}$. Since $F_{j-\frac{1}{2}} > 0$ and $F_{j+\frac{1}{2}} < 0$, we have $0 < -\frac{F_{j+\frac{1}{2}}}{\lambda F_{j-\frac{1}{2}} - \lambda F_{j+\frac{1}{2}}} \leq 1/\lambda$. Recalling

$$\Gamma_j^M - (\lambda F_{j-\frac{1}{2}} - \lambda F_{j+\frac{1}{2}}) = u_M - \{u_j - \lambda(\hat{H}_{j+\frac{1}{2}}^{rk} - \hat{H}_{j-\frac{1}{2}}^{rk})\} < 0, \quad (3.7)$$

it suffices to show

$$|u_M - \{u_j - \lambda(\hat{H}_{j+\frac{1}{2}}^{rk} - \hat{H}_{j-\frac{1}{2}}^{rk})\}| = \mathcal{O}(\Delta x^3 + \Delta t^3). \quad (3.8)$$

Equation (3.8) can be justified by using equation (3.4), since in this case we have $u(x_j, t^{n+1}) \leq u_M \leq u_j^{n+1}$, where $u_j^{n+1} = u_j - \lambda(\hat{H}_{j+\frac{1}{2}}^{rk} - \hat{H}_{j-\frac{1}{2}}^{rk})$.

Case (b): Similar to case (d), we only need to consider the case when

$$\Lambda_{+\frac{1}{2}, I_j} = \frac{\Gamma_j^M}{-\lambda F_{j+\frac{1}{2}}} < 1. \quad (3.9)$$

with

$$\tilde{H}_{j+\frac{1}{2}}^{rk} - \hat{H}_{j+\frac{1}{2}}^{rk} = \frac{\Gamma_j^M + \lambda F_{j+\frac{1}{2}}}{-\lambda} = \frac{u_M - (u_j - \lambda(\hat{H}_{j+\frac{1}{2}}^{rk} - \hat{h}_{j-\frac{1}{2}}))}{-\lambda}. \quad (3.10)$$

To prove (3.5), it suffices to prove

$$|u_M - (u_j - \lambda(\hat{H}_{j+\frac{1}{2}}^{rk} - \hat{h}_{j-\frac{1}{2}}))| = \mathcal{O}(\Delta x^3 + \Delta t^3), \quad (3.11)$$

if $u_M - (u_j - \lambda(\hat{H}_{j+\frac{1}{2}}^{rk} - \hat{h}_{j-\frac{1}{2}})) < 0$. For the high order RK flux, we have

$$\hat{H}_{j+\frac{1}{2}}^{rk} = \frac{1}{\Delta t} \int_{t^n}^{t^{n+1}} h(x_{j+\frac{1}{2}}, t) dt + \mathcal{O}(\Delta t^3). \quad (3.12)$$

Using the 3-point Gauss Lobatto quadrature for (3.12), we can get

$$\frac{1}{\Delta t} \int_{t^n}^{t^{n+1}} h(x_{j+\frac{1}{2}}, t) dt = \frac{1}{6} h(x_{j+\frac{1}{2}}, t^n + \Delta t) + \frac{2}{3} h(x_{j+\frac{1}{2}}, t^n + \frac{\Delta t}{2}) + \frac{1}{6} h(x_{j+\frac{1}{2}}, t^n) + \mathcal{O}(\Delta t^3). \quad (3.13)$$

The sliding average function h can be given in the following expanded form [9]

$$h(x_{j+\frac{1}{2}}, t) = f(u(x_{j+\frac{1}{2}}, t)) + \sum_{k=1}^s a_{2k} \Delta x^{2k} \left(\frac{\partial^{2k}}{\partial x^{2k}} f(u(x, t)) \right)_{x=x_{j+\frac{1}{2}}} + \mathcal{O}(\Delta x^{2s+2}) \quad (3.14)$$

with properly defined $\{a_{2k}\}$ to ensure $(h(x_{j+\frac{1}{2}}, t) - h(x_{j-\frac{1}{2}}, t))/\Delta x = f(u)_x(x_j, t) + \mathcal{O}(\Delta x^{2s+1})$ for arbitrary s . For a third order approximation, taking the first two terms in (3.14) and approximating $f_{xx}(u)$ by a central difference, we have

$$h(x_{j+\frac{1}{2}}, t) = f(u(x_{j+\frac{1}{2}}, t)) - \frac{\Delta x^2}{24} f_{xx}(u(x_{j+\frac{1}{2}}, t)) + \mathcal{O}(\Delta x^4) \quad (3.15)$$

$$= \frac{13}{12} f(u(x_{j+\frac{1}{2}}, t)) - \frac{1}{24} (f(u(x_{j+\frac{3}{2}}, t)) + f(u(x_{j-\frac{1}{2}}, t))) + \mathcal{O}(\Delta x^4). \quad (3.16)$$

Now (3.13) can be written as

$$\begin{aligned} & \frac{1}{\Delta t} \int_{t^n}^{t^{n+1}} h(x_{j+\frac{1}{2}}, t) dt \\ &= \frac{1}{6} \left(\frac{13}{12} f(u(x_{j+\frac{1}{2}}, t^n + \Delta t)) - \frac{1}{24} (f(u(x_{j+\frac{3}{2}}, t^n + \Delta t)) + f(u(x_{j-\frac{1}{2}}, t^n + \Delta t))) \right) \\ & \quad + \frac{2}{3} \left(\frac{13}{12} f(u(x_{j+\frac{1}{2}}, t^n + \frac{\Delta t}{2})) - \frac{1}{24} (f(u(x_{j+\frac{3}{2}}, t^n + \frac{\Delta t}{2})) + f(u(x_{j-\frac{1}{2}}, t^n + \frac{\Delta t}{2}))) \right) \\ & \quad + \frac{1}{6} \left(\frac{13}{12} f(u(x_{j+\frac{1}{2}}, t^n)) - \frac{1}{24} (f(u(x_{j+\frac{3}{2}}, t^n)) + f(u(x_{j-\frac{1}{2}}, t^n))) \right) + \mathcal{O}(\Delta t^3 + \Delta x^4). \end{aligned}$$

Following the characteristics, we have

$$\begin{aligned} & \frac{1}{\Delta t} \int_{t^n}^{t^{n+1}} h(x_{j+\frac{1}{2}}, t) dt \\ &= \frac{1}{6} \left(\frac{13}{12} f(u(x_{j+\frac{1}{2}} - \lambda_{21} \Delta x, t^n)) - \frac{1}{24} (f(u(x_{j+\frac{3}{2}} - \lambda_{31} \Delta x, t^n)) + f(u(x_{j-\frac{1}{2}} - \lambda_{11} \Delta x, t^n))) \right) \\ & \quad + \frac{2}{3} \left(\frac{13}{12} f(u(x_{j+\frac{1}{2}} - \lambda_{22} \Delta x, t^n)) - \frac{1}{24} (f(u(x_{j+\frac{3}{2}} - \lambda_{32} \Delta x, t^n)) + f(u(x_{j-\frac{1}{2}} - \lambda_{12} \Delta x, t^n))) \right) \\ & \quad + \frac{1}{6} \left(\frac{13}{12} f(u(x_{j+\frac{1}{2}}, t^n)) - \frac{1}{24} (f(u(x_{j+\frac{3}{2}}, t^n)) + f(u(x_{j-\frac{1}{2}}, t^n))) \right) + \mathcal{O}(\Delta t^3 + \Delta x^4) \quad (3.17) \end{aligned}$$

where

$$\lambda_{11} = \lambda f'(u(x_{j-\frac{1}{2}} - \lambda_{11} \Delta x, t^n)), \quad \lambda_{12} = \frac{\lambda}{2} f'(u(x_{j-\frac{1}{2}} - \lambda_{12} \Delta x, t^n)), \quad (3.18)$$

$$\lambda_{21} = \lambda f'(u(x_{j+\frac{1}{2}} - \lambda_{21} \Delta x, t^n)), \quad \lambda_{22} = \frac{\lambda}{2} f'(u(x_{j+\frac{1}{2}} - \lambda_{22} \Delta x, t^n)), \quad (3.19)$$

$$\lambda_{31} = \lambda f'(u(x_{j+\frac{3}{2}} - \lambda_{31} \Delta x, t^n)), \quad \lambda_{32} = \frac{\lambda}{2} f'(u(x_{j+\frac{3}{2}} - \lambda_{32} \Delta x, t^n)). \quad (3.20)$$

We prove (3.11) case by case. For the high order flux, we approximate $f(u(x, t^n))$ in (3.17) by a third order polynomial interpolating $f(u_{j-1})$, $f(u_j)$ and $f(u_{j+1})$. We take the local Lax-Friedrichs (LLF) flux as the first order monotone flux $\hat{h}_{j-\frac{1}{2}} = \frac{1}{2}(f(u_j) + f(u_{j-1})) - \alpha_{j-\frac{1}{2}}(u_j - u_{j-1})$, where $\alpha_{j-\frac{1}{2}} = \max_{u \in [A, B]} |f'(u)|$ with $A = \min\{u_{j-1}, u_j\}$ and $B = \max\{u_{j-1}, u_j\}$.

We first consider the case $x_M \in I_j$, with $u_M = u(x_M)$, $u'_M = 0$ and $u''_M \leq 0$. We perform Taylor expansions around x_M

$$u_j = u_M + u'_M(x_j - x_M) + u''_M \frac{(x_j - x_M)^2}{2} + O(\Delta x^3) \quad (3.21)$$

$$f(u_j) = f(u_M) + f'(u_M)u'_M(x_j - x_M) + (f'(u_M)u''_M + f''(u_M)(u'_M)^2) \frac{(x_j - x_M)^2}{2} + O(\Delta x^3) \quad (3.22)$$

$$f(u_{j-1}) = f(u_M) + f'(u_M)u'_M(x_j - x_M - \Delta x) + (f'(u_M)u''_M + f''(u_M)(u'_M)^2) \frac{(x_j - x_M - \Delta x)^2}{2} + O(\Delta x^3) \quad (3.23)$$

$$f(u_{j+1}) = f(u_M) + f'(u_M)u'_M(x_j - x_M + \Delta x) + (f'(u_M)u''_M + f''(u_M)(u'_M)^2) \frac{(x_j - x_M + \Delta x)^2}{2} + O(\Delta x^3) \quad (3.24)$$

If we denote $\lambda_{k,1} = \lambda_0 + \eta_{k,1}\Delta x + \mathcal{O}(\Delta x^2)$ and $\lambda_{k,2} = \frac{\lambda_0}{2} + \zeta_{k,2}\Delta x + \mathcal{O}(\Delta x^2)$ for $k = 1, 2, 3$, where $\lambda_0 = \lambda f'(u_M)$, substitute into (3.18)-(3.20) to determine $\eta_{k,1}$ and $\zeta_{k,2}$, we have

$$\begin{aligned} \lambda_{11} &= \lambda_0 + f''(u_M)u'_M \lambda \left(z - \frac{1}{2} - \lambda_0\right) \Delta x + \mathcal{O}(\Delta x^2), \\ \lambda_{12} &= \frac{\lambda_0}{2} + f''(u_M)u'_M \frac{\lambda}{2} \left(z - \frac{1}{2} - \frac{\lambda_0}{2}\right) \Delta x + \mathcal{O}(\Delta x^2), \\ \lambda_{21} &= \lambda_0 + f''(u_M)u'_M \lambda \left(z + \frac{1}{2} - \lambda_0\right) \Delta x + \mathcal{O}(\Delta x^2), \\ \lambda_{22} &= \frac{\lambda_0}{2} + f''(u_M)u'_M \frac{\lambda}{2} \left(z + \frac{1}{2} - \frac{\lambda_0}{2}\right) \Delta x + \mathcal{O}(\Delta x^2), \\ \lambda_{31} &= \lambda_0 + f''(u_M)u'_M \lambda \left(z + \frac{3}{2} - \lambda_0\right) \Delta x + \mathcal{O}(\Delta x^2), \\ \lambda_{32} &= \frac{\lambda_0}{2} + f''(u_M)u'_M \frac{\lambda}{2} \left(z + \frac{3}{2} - \frac{\lambda_0}{2}\right) \Delta x + \mathcal{O}(\Delta x^2). \end{aligned}$$

with $z = (x_j - x_M)/\Delta x$.

With above notation and $u'_M = 0$, we have

$$u_j - \lambda \left(\frac{1}{\Delta t} \int_{t^n}^{t^{n+1}} h(x_{j+\frac{1}{2}}, t) dt - \hat{h}_{j-\frac{1}{2}} \right) = u_M + \frac{u''_M}{12} \Delta x^2 g(z, \lambda_0) + \mathcal{O}(\Delta x^3 + \Delta t^3) \quad (3.25)$$

with

$$g(z, \lambda_0) = (3\alpha_{j-\frac{1}{2}}\lambda + 2\lambda_0 + 3\lambda_0^2 - 2\lambda_0^3) + 6(-\alpha_{j-\frac{1}{2}}\lambda - 2\lambda_0 + \lambda_0^2)z + 6z^2 \quad (3.26)$$

We discuss $g(z, \lambda_0)$ with the following two cases:

- If $f'(u_M) \geq 0$, we have $\lambda_0 = \lambda f'(u_M) \in [0, 1]$ since $\lambda \max_u |f'(u)| \leq 1$, and we can write $g(z, \lambda_0)$ to be

$$g(z, \lambda_0) = g_1(z, \lambda_0) + 6(\alpha_{j-\frac{1}{2}}\lambda - \lambda_0)\left(\frac{1}{2} + z\right) \quad (3.27)$$

with

$$g_1(z, \lambda_0) = (5\lambda_0 + 3\lambda_0^2 - 2\lambda_0^3) + 6(-3\lambda_0 + \lambda_0^2)z + 6z^2 \quad (3.28)$$

the minimum value of function g_1 with respect to z is

$$(g_1)_{min} = g_1(z, \lambda_0) \Big|_{z=-\frac{1}{2}\lambda_0(\lambda_0-3)} = \frac{\lambda_0}{2}(\lambda_0 - 2)(\lambda_0 - 1)(5 - 3\lambda_0) \geq 0 \quad (3.29)$$

and since $|\alpha_{j-\frac{1}{2}} - f'(u_M)| = \mathcal{O}(\Delta x)$, we have $|(\alpha_{j-\frac{1}{2}}\lambda - \lambda_0)(\frac{1}{2} + z)| = |\lambda(\frac{1}{2} + z)||\alpha_{j-\frac{1}{2}} - f'(u_M)| = \mathcal{O}(\Delta x)$, that is $g(z, \lambda_0) = g_1(z, \lambda_0) + \mathcal{O}(\Delta x)$ with $g_1(z, \lambda_0) \geq 0$. Since $u_M'' \leq 0$, we obtain (3.11).

- If $f'(u_M) < 0$, we have $\lambda_0 \in [-1, 0]$, similarly we have

$$g(z, \lambda_0) = g_2(z, \lambda_0) + 6(\alpha_{j-\frac{1}{2}}\lambda + \lambda_0)(\frac{1}{2} + z) \quad (3.30)$$

with

$$g_2(z, \lambda_0) = (-\lambda_0 + 3\lambda_0^2 - 2\lambda_0^3) + 6(-\lambda_0 + \lambda_0^2)z + 6z^2 \quad (3.31)$$

the minimum value of g_2 with respect to z is

$$(g_2)_{min} = g_2(z, \lambda_0) \Big|_{z=-\frac{1}{2}\lambda_0(\lambda_0-1)} = \frac{\lambda_0}{2}(\lambda_0 + 1)(\lambda_0 - 1)(2 - 3\lambda_0) \geq 0 \quad (3.32)$$

and similarly $|(\alpha_{j-\frac{1}{2}}\lambda + \lambda_0)(\frac{1}{2} + z)| = \mathcal{O}(\Delta x)$, we get $g(z, \lambda_0) = g_2(z, \lambda_0) + \mathcal{O}(\Delta x)$ with $g_2(z, \lambda_0) \geq 0$. Since $u_M'' \leq 0$, we also obtain (3.11).

Now if $x_M \notin I_j$, however there is a local maximum point x_M^{loc} inside the cell of I_j , the above analysis still holds. We therefore consider that $u(x)$ reaches its local maximum u_M^{loc} over I_j at $x_M^{loc} = x_{j-\frac{1}{2}}$, we have $u'_{j-\frac{1}{2}} < 0$. From the Taylor expansions in (3.21)-(3.24), following the same procedure as above, with $z = (x_j - x_M^{loc})/\Delta x = (x_j - x_{j-\frac{1}{2}})/\Delta x = 1/2$, we have

$$\begin{aligned} u_j &= \lambda \left(\frac{1}{\Delta t} \int_{t^n}^{t^{n+1}} h(x_{j+\frac{1}{2}}, t) dt - \hat{h}_{j-\frac{1}{2}} \right) \\ &= u_{j-\frac{1}{2}} + u'_{j-\frac{1}{2}} \Delta x s_1 + (u'_{j-\frac{1}{2}})^2 \Delta x^2 s_2 + u''_{j-\frac{1}{2}} \frac{\Delta x^2}{2} s_3 + \mathcal{O}(\Delta x^3 + \Delta t^3) \end{aligned} \quad (3.33)$$

where

$$\begin{aligned} s_1 &= \frac{1}{2}(1 - 2\lambda_0 + \lambda_0^2) - \frac{\lambda}{2}\alpha_{j-\frac{1}{2}} \\ s_2 &= -f''(u_{j-\frac{1}{2}}) \frac{\lambda}{6}(2 - 6\lambda_0 + 3\lambda_0^2) \\ s_3 &= \frac{1}{12}(3 - 8\lambda_0 + 12\lambda_0^2 - 4\lambda_0^3) \end{aligned}$$

If $f'(u_{j-\frac{1}{2}}) \geq 0$, we have $\alpha_{j-\frac{1}{2}} - f'(u_{j-\frac{1}{2}}) = \mathcal{O}(\Delta x)$ and $\lambda_0 \in [0, 1]$. We can write (3.33) to be

$$\begin{aligned} u_j &= \lambda \left(\frac{1}{\Delta t} \int_{t^n}^{t^{n+1}} h(x_{j+\frac{1}{2}}, t) dt - \hat{h}_{j-\frac{1}{2}} \right) \\ &= u(x_{j-\frac{1}{2}} - \sqrt{s_3} \Delta x) + u'_{j-\frac{1}{2}} \Delta x \left(\frac{1}{2}(1 - 3\lambda_0 + \lambda_0^2) + \sqrt{s_3} \right) + u'_{j-\frac{1}{2}} \Delta x^2 s_4 \\ &\quad + \mathcal{O}(\Delta x^3 + \Delta t^3) \end{aligned} \quad (3.34)$$

where $s_4 = u'_{j-\frac{1}{2}} s_2 - \frac{\lambda}{2} \frac{\alpha_{j-\frac{1}{2}} - f'(u_{j-\frac{1}{2}})}{\Delta x}$, which is in the order of $\mathcal{O}(1)$. It is easy to check that $s_3 \geq 0$ and $\frac{1}{2}(1 - 3\lambda_0 + \lambda_0^2) + \sqrt{s_3} \geq 0$.

However, if $f'(u_{j-\frac{1}{2}}) < 0$ and $\lambda_0 \in [-1, 0]$. We can write (3.33) as

$$\begin{aligned} u_j &= \lambda \left(\frac{1}{\Delta t} \int_{t^n}^{t^{n+1}} h(x_{j+\frac{1}{2}}, t) dt - \hat{h}_{j-\frac{1}{2}} \right) \\ &= u(x_{j-\frac{1}{2}} - \sqrt{s_3} \Delta x) + u'_{j-\frac{1}{2}} \Delta x (s_1 + \sqrt{s_3}) + u'_{j-\frac{1}{2}} \Delta x^2 s_4 \\ &\quad + \mathcal{O}(\Delta x^3 + \Delta t^3) \end{aligned} \quad (3.35)$$

where $s_4 = u'_{j-\frac{1}{2}} s_2$. $s_3 \geq 0$, $s_1 + \sqrt{s_3} \geq 0$ for $\lambda_0 \in [-1, 0]$ and $\lambda \alpha_{j-\frac{1}{2}} \leq 1$.

In the above two cases, to prove (3.11), it is sufficient to show $u(x_{j-\frac{1}{2}} - \sqrt{s_3} \Delta x) + \Delta x^2 u'_{j-\frac{1}{2}} s_4 \leq u_M$ or $u'_{j-\frac{1}{2}} = \mathcal{O}(\Delta x)$. If $[x_{j-\frac{1}{2}} - \sqrt{s_3} \Delta x - \Delta x, x_{j-\frac{1}{2}} - \sqrt{s_3} \Delta x]$ is not a monotone region, there is a point $x^{\#,1}$ in this region, such that $u'(x^{\#,1}) = 0$. Similarly, if $[x_{j-\frac{1}{2}} - \sqrt{s_3} \Delta x - \Delta x, x_{j-\frac{1}{2}} - \sqrt{s_3} \Delta x]$ is a monotone increasing region, since $u'_{j-\frac{1}{2}} < 0$, there is one point $x^{\#,2}$ in $[x_{j-\frac{1}{2}} - \sqrt{s_3} \Delta x, x_{j-\frac{1}{2}}]$, such that $u'(x^{\#,2}) = 0$. For these two cases, $u'_{j-\frac{1}{2}} = \mathcal{O}(\Delta x)$. We then focus on the case when $[x_{j-\frac{1}{2}} - \sqrt{s_3} \Delta x - \Delta x, x_{j-\frac{1}{2}} - \sqrt{s_3} \Delta x]$ is a monotone decreasing region. We assume

$$u(x_{j-\frac{1}{2}} - \sqrt{s_3} \Delta x) + c \Delta x^2 > u_M$$

where $c = |u'_{j-\frac{1}{2}} s_4|$. Since

$$u(x_{j-\frac{1}{2}} - \sqrt{s_3} \Delta x) = u(x_{j-\frac{1}{2}} - \sqrt{s_3} \Delta x - \Delta x) + u'(x^{\#,3}) \Delta x,$$

where $u'(x^{\#,3}) < 0$, we have

$$u'(x^{\#,3}) \Delta x + c \Delta x^2 > 0,$$

which implies $|u'(x^{\#,3})| \leq c \Delta x$, therefore, $u'_{j-\frac{1}{2}} = \mathcal{O}(\Delta x)$.

$x_M^{loc} = x_{j+\frac{1}{2}}$ with $u'(x_M^{loc}) \geq 0$ can be proved similarly. Combining the above discussion, (3.11) is proved. \square

Remark 3.3. From Theorem 3.2, we have proved that the proposed MPP flux limiter with LLF fluxes as the first order monotone fluxes introduces a third order modification to the original RK fluxes $\hat{H}_{j+\frac{1}{2}}^{rk}$ for a third order finite difference scheme without additional time step restriction. When Godunov flux is used as the first order monotone flux, the same conclusion holds. However, when global Lax-Friedrichs (LF) flux is used as the first order monotone flux, additional time step restriction would be needed, as $s_1 + \sqrt{s_3}$ is not always positive in (3.33) when $f'(u_{j-\frac{1}{2}}) \geq 0$ (see the form (3.35)). However, under a smaller CFL number, i.e., $\lambda\alpha = \lambda \max_u |f'(u)| \leq 0.886$, $s_1 + \sqrt{s_3} \geq 0$ in (3.33), thus the 3rd order accuracy is maintained. Extension of the above analysis to higher order case would be very technical and algebraically complicated and is out of the scope of the current paper.

3.2 Two-dimensional problem

We consider the two-dimensional scalar problem

$$u_t + f(u)_x + g(u)_y = 0, \quad u(x, y, 0) = u_0(x, y). \quad (3.36)$$

The multi-dimensional parametrized MPP flux limiters for high order schemes solving (3.36) are developed in [15]. We refer to [15] for the algorithm description and implementation details of the successive MPP flux limiters for multi-dimensional problems. In this section, we would like to apply the MPP flux limiters at the final stage of the multi-stage RK-WENO schemes solving two-dimensional problem (3.36). As in the one-dimensional case, the high order finite difference RK-WENO scheme can be written as

$$u_{i,j}^{n+1} = u_{i,j}^n - \lambda_x (\hat{H}_{i+1/2,j}^{rk} - \hat{H}_{i-1/2,j}^{rk}) - \lambda_y (\hat{G}_{i,j+1/2}^{rk} - \hat{G}_{i,j-1/2}^{rk}), \quad (3.37)$$

where \hat{H}^{rk} and \hat{G}^{rk} are linear combination of fluxes from RK multiple stages. Let $\hat{h}_{i+1/2,j}$, $\hat{g}_{i,j+1/2}$ be any first order monotone flux satisfying maximum principle,

$$u_m \leq u_{i,j}^n - \lambda_x (\hat{h}_{i+1/2,j} - \hat{h}_{i-1/2,j}) - \lambda_y (\hat{g}_{i,j+1/2} - \hat{g}_{i,j-1/2}) \leq u_M. \quad (3.38)$$

In order to ensure maximum principle, we are looking for the type of limiters

$$\begin{aligned} \tilde{H}_{i+1/2,j} &= \theta_{i+1/2,j} (\hat{H}_{i+1/2,j}^{rk} - \hat{h}_{i+1/2,j}) + \hat{h}_{i+1/2,j}, \\ \tilde{G}_{i,j+1/2} &= \theta_{i,j+1/2} (\hat{G}_{i,j+1/2}^{rk} - \hat{g}_{i,j+1/2}) + \hat{g}_{i,j+1/2} \end{aligned} \quad (3.39)$$

such that

$$u_m \leq u_{i,j}^n - \lambda_x (\tilde{H}_{i+1/2,j} - \tilde{H}_{i-1/2,j}) - \lambda_y (\tilde{G}_{i,j+1/2} - \tilde{G}_{i,j-1/2}) \leq u_M. \quad (3.40)$$

(3.39) and (3.40) form coupled inequalities for the limiting parameters $\theta_{i+1/2,j}, \theta_{i,j+1/2}$. As for the 1-D case, for each node (i, j) , the maximum principle preserving limiters can be parametrized in the sense that we can find a group of numbers $\Lambda_{L,i,j}, \Lambda_{R,i,j}, \Lambda_{D,i,j}, \Lambda_{U,i,j}$, such that the numerical solutions of (3.37) satisfy the MPP property (3.40) with

$$(\theta_{i-1/2,j}, \theta_{i+1/2,j}, \theta_{i,j-1/2}, \theta_{i,j+1/2}) \in [0, \Lambda_{L,i,j}] \times [0, \Lambda_{R,i,j}] \times [0, \Lambda_{D,i,j}] \times [0, \Lambda_{U,i,j}].$$

For the maximum value case, let

$$\Gamma_{i,j} = u_M - (u_{i,j} - \lambda_x(\hat{h}_{i+1/2,j} - \hat{h}_{i-1/2,j}) - \lambda_y(\hat{g}_{i,j+1/2} - \hat{g}_{i,j-1/2})) \geq 0, \quad (3.41)$$

when a monotone numerical flux is used under suitable CFL constraint $\alpha_x \frac{\Delta t}{\Delta x} + \alpha_y \frac{\Delta t}{\Delta y} \leq 1$, here $\alpha_x = \max_u |f'(u)|$ and $\alpha_y = \max_u |g'(u)|$. Denote

$$\begin{cases} F_{i-1/2,j} = \lambda_x(\hat{H}_{i-1/2,j}^{rk} - \hat{h}_{i-1/2,j}), \\ F_{i+1/2,j} = -\lambda_x(\hat{H}_{i+1/2,j}^{rk} - \hat{h}_{i+1/2,j}), \\ F_{i,j-1/2} = \lambda_y(\hat{G}_{i,j-1/2}^{rk} - \hat{g}_{i,j-1/2}), \\ F_{i,j+1/2} = -\lambda_y(\hat{G}_{i,j+1/2}^{rk} - \hat{g}_{i,j+1/2}). \end{cases} \quad (3.42)$$

The coupled inequalities (3.39) and (3.40) can be rewritten as

$$\theta_{i+1/2,j}F_{i+1/2,j} + \theta_{i-1/2,j}F_{i-1/2,j} + \theta_{i,j+1/2}F_{i,j+1/2} + \theta_{i,j-1/2}F_{i,j-1/2} \leq \Gamma_{i,j}, \quad (3.43)$$

We shall now focus on decoupling the inequalities (3.43). For the single node (i, j) ,

1. Identify positive values out of the four locally defined numbers $F_{i-1/2,j}, F_{i+1/2,j}, F_{i,j-1/2}, F_{i,j+1/2}$;
2. Corresponding to those positive values, **collectively**, the limiting parameters can be defined. For example, if $F_{i+1/2,j}, F_{i-1/2,j} > 0$ and $F_{i,j-1/2}, F_{i,j+1/2} \leq 0$, then

$$\begin{cases} \Lambda_{i+1/2,j}^M, \Lambda_{i-1/2,j}^M = \min\left(\frac{\Gamma_{i,j}}{F_{i+1/2,j} + F_{i-1/2,j}}, 1\right), \\ \Lambda_{i,j-1/2}^M, \Lambda_{i,j+1/2}^M = 1. \end{cases} \quad (3.44)$$

For the minimum value part, let

$$\Gamma_{i,j} = u_m - (u_{i,j} - \lambda_x(\hat{h}_{i+1/2,j} - \hat{h}_{i-1/2,j}) - \lambda_y(\hat{g}_{i,j+1/2} - \hat{g}_{i,j-1/2})) \leq 0. \quad (3.45)$$

The coupled inequalities (3.39) and (3.40) can be rewritten as

$$\Gamma_{i,j} \leq \theta_{i+1/2,j}F_{i+1/2,j} + \theta_{i-1/2,j}F_{i-1/2,j} + \theta_{i,j+1/2}F_{i,j+1/2} + \theta_{i,j-1/2}F_{i,j-1/2}. \quad (3.46)$$

A similar procedure would be applied

1. Identify negative values out of the four locally defined numbers $F_{i-1/2,j}$, $F_{i+1/2,j}$, $F_{i,j-1/2}$, $F_{i,j+1/2}$;
2. Corresponding to the negative values, **collectively**, the limiting parameters can be defined. For example, if $F_{i,j-1/2}, F_{i,j+1/2} \geq 0$ and $F_{i-1/2,j}, F_{i+1/2,j} < 0$, then

$$\begin{cases} \Lambda_{i-1/2,j}^m, \Lambda_{i+1/2,j}^m = \min\left(\frac{\Gamma_{i,j}}{F_{i-1/2,j} + F_{i+1/2,j}}, 1\right) \\ \Lambda_{i,j-1/2}^m, \Lambda_{i,j+1/2}^m = 1. \end{cases} \quad (3.47)$$

Namely, all high order fluxes which possibly contribute (beyond that of the first order fluxes) to the overshooting or undershooting of the updated value shall be limited by the same scaling. Similarly we can find $\Lambda_{i,j\pm 1/2}^M$ and $\Lambda_{i,j\pm 1/2}^m$. The range of the limiting parameters satisfying MPP for a single node (i, j) therefore can be defined by

$$\begin{cases} \Lambda_{L,i,j} = \min(\Lambda_{i-1/2,j}^M, \Lambda_{i-1/2,j}^m), \\ \Lambda_{R,i,j} = \min(\Lambda_{i+1/2,j}^M, \Lambda_{i+1/2,j}^m), \\ \Lambda_{U,i,j} = \min(\Lambda_{i,j+1/2}^M, \Lambda_{i,j+1/2}^m), \\ \Lambda_{D,i,j} = \min(\Lambda_{i,j-1/2}^M, \Lambda_{i,j-1/2}^m). \end{cases} \quad (3.48)$$

Considering the limiters from neighboring nodes, finally we let

$$\begin{cases} \theta_{i+1/2,j} = \min(\Lambda_{R,i,j}, \Lambda_{L,i+1,j}), \\ \theta_{i,j+1/2} = \min(\Lambda_{U,i,j}, \Lambda_{D,i,j+1}). \end{cases} \quad (3.49)$$

The flux limiters designed for two-dimensional problem (3.36) can be easily generalized to higher dimensional problems. The analytical tools in performing Taylor expansions, handling the sliding average functions and in tracing characteristics in proving Theorem 3.2 can be generalized for 2-D problems. However, in our current approach, more algebraic computations are needed for schemes of higher orders and for problems of higher dimensions. It is our future work to find a general approach in investigating the maintenance of high order spatial and temporal accuracy, without a case-specific discussion.

4 The MPP flux limiter for incompressible flow

Consider 2D equations describing advection in incompressible flow,

$$u_t + (v_1(x, y, t)u)_x + (v_2(x, y, t)u)_y = 0, \quad (4.1)$$

in conservative form with the divergence free condition of the velocity field

$$\nabla_{\mathbf{x}} \cdot \mathbf{v} = 0. \quad (4.2)$$

The solutions of such equation enjoy the properties of mass conservation and strict maximum principle thanks to the divergence-free condition. The challenge of computing (4.1) by a conservative scheme is to preserve a discrete divergence-free condition, especially when a high order method is used. In this section, we start from introducing a first order monotone scheme in flux difference form which is in a similar spirit to that discussed in [3]. With the divergence-free condition, there exists a potential function Φ , s.t. $\mathbf{v} = (-\Phi_y, \Phi_x)^T$. In some cases, when the analytical formulae of the potential function is hard to be determined from v_1 and v_2 , it can be computed through solving the Poisson equation

$$\Delta\Phi = -\partial_y v_1 + \partial_x v_2 \quad (4.3)$$

with a stable scheme, i.e., a five-point central difference scheme. The previously computed discrete values of the potential function can be used to design the following first order monotone scheme. Assuming

$$\begin{aligned} \alpha_{i-1,j} &= -\frac{\Delta t}{\Delta x \Delta y} (\Phi_{i-1,j} - \Phi_{i-1,j-1}) \geq 0, \\ \alpha_{i,j-1} &= \frac{\Delta t}{\Delta x \Delta y} (\Phi_{i,j-1} - \Phi_{i-1,j-1}) \geq 0, \end{aligned}$$

Let $D_x^\pm \Phi_{i,j} = \pm(\Phi_{i\pm 1,j} - \Phi_{i,j})$ and $D_y^\pm \Phi_{i,j} = \pm(\Phi_{i,j\pm 1} - \Phi_{i,j})$. The first order monotone scheme is designed by using the potential function Φ :

$$\begin{aligned} u_{i,j}^{n+1} &= u_{i,j}^n - \Delta t \left(-D_x^-((D_y^- \Phi)u^n) + D_y^-((D_x^- \Phi)u^n) \right) \\ &= \alpha_{i,j} u_{i,j}^n + \alpha_{i-1,j} u_{i-1,j}^n + \alpha_{i,j-1} u_{i,j-1}^n \end{aligned} \quad (4.4)$$

with

$$\alpha_{i,j} = 1 - (\alpha_{i-1,j} + \alpha_{i,j-1}).$$

These coefficients α are positive under the CFL condition $\alpha_x \frac{\Delta t}{\Delta x} + \alpha_y \frac{\Delta t}{\Delta y} \leq 1$, here $\alpha_x = \max |D_y^- \Phi| / \Delta y$ and $\alpha_y = \max |D_x^- \Phi| / \Delta x$. With the updated solution being the convex combination of the solution from previous time steps, it is easy to check that the first order scheme (4.4) satisfies the MPP property.

For the general case, we perform a flux splitting of Φ . For example, with the Lax-Friedrichs splitting, we let

$$\Phi^+ = \frac{1}{2} (\Phi + \alpha_x x + \alpha_y y), \quad \Phi^- = \frac{1}{2} (\Phi - (\alpha_x x + \alpha_y y)) \quad (4.5)$$

with α_x and α_y large enough, so that $D_x^-(\Phi^+) \geq 0$, $D_y^-(\Phi^+) \geq 0$, $D_x^+(\Phi^-) \leq 0$ and $D_y^+(\Phi^-) \leq 0$. A first order monotone scheme satisfying the MPP property can be designed as

$$\begin{aligned} u_{i,j}^{n+1} = & u_{i,j}^n - \Delta t \left(D_x^+((-D_y^-\Phi^+)u^n) + D_x^-((-D_y^+\Phi^-)u^n) \right. \\ & \left. + D_y^-((D_x^+\Phi^+)u^n) + D_y^+((D_x^-\Phi^-)u^n) \right). \end{aligned} \quad (4.6)$$

Similar to equation (4.4), it is easy to check that the scheme (4.6) satisfies the MPP property.

Similar to the MPP flux limiters presented in Section 3, the high order finite difference RK-WENO scheme for the conservative form of incompressible flow (4.1) can be written in the form of (3.37) with the MPP flux limiter (3.39), where

$$\begin{aligned} \hat{h}_{i+\frac{1}{2},j} = & -\frac{\Phi_{i+1,j} - \Phi_{i+1,j-1}}{2\Delta y} u_{i+1,j} - \frac{\Phi_{i,j+1} - \Phi_{i,j}}{2\Delta y} u_{i,j} - \frac{\alpha_x}{2} (u_{i+1,j} - u_{i,j}) \\ \hat{g}_{i,j+\frac{1}{2}} = & \frac{\Phi_{i+1,j} - \Phi_{i,j}}{2\Delta x} u_{i,j} + \frac{\Phi_{i,j+1} - \Phi_{i-1,j+1}}{2\Delta x} u_{i,j+1} - \frac{\alpha_y}{2} (u_{i,j+1} - u_{i,j}) \end{aligned}$$

is the numerical flux from the first order scheme (4.6) with MPP property.

The application of the high order FD RK-WENO scheme with general MPP flux limiters presented in the previous sections to the incompressible flow problem is convenient based on the above description. However, a rigorous justification on maintenance of high order accuracy, following the line of proof for the third order scheme solving advection equation, is technically prohibitive due to the increased complexity of the flux function and tracing of the characteristic etc. A thorough analysis will be part of our future investigation.

Remark 4.1. The computation of incompressible flow can also be applied to the incompressible Euler equations with vorticity stream-function formulation in the form (5.7) and (5.8). In this case, we solve the potential function from the Poisson equation by the Fourier spectral method.

5 Numerical simulations

5.1 Basic tests.

In this section, we present numerical examples for the proposed parametrized MPP flux limiters for high order finite difference schemes with high order RK time discretization. There are two schemes we tested. One is the 3rd order finite difference scheme with 3rd order Runge-Kutta time discretization, denote as ‘‘FD3RK3’’, here the 3rd order finite difference scheme is the 3rd order finite difference WENO scheme but with linear weights; the other is the 5th

order finite difference WENO scheme with 4th order RK time discretization [8] denoted as “WENO5RK4”. We use the global Lax-Friedrichs scheme as the first order monotone scheme, unless otherwise stated. And the CFL condition in our numerical experiments is defined to be $\max_u |f'(u)| \frac{\Delta t}{\Delta x} \leq CFL$ for one dimensional case, and $\max_u |f'(u)| \frac{\Delta t}{\Delta x} + \max_u |g'(u)| \frac{\Delta t}{\Delta y} \leq CFL$ for two dimensional case.

Example 5.1. Consider the 1D linear equation

$$u_t + u_x = 0, \quad u(x, 0) = u_0(x) \quad (5.1)$$

on $[0, 2\pi]$ with periodic boundary conditions. We take the initial condition to be $u_0(x) = \sin^4(x)$. We list the L^1 and L^∞ errors at $T = 0.5$ in Tables 5.1-5.4 with $CFL = 0.6$. The 3rd order for “FD3RK3” and 5th order for “WENO5RK4” schemes with the MPP flux limiters are numerically observed. The minimum values are observed to be strictly non-negative from schemes with limiters. We also test $CFL = 1.0$ for “FD3RK3” and report results in Tables 5.5-5.6. Similar behaviors are observed.

Table 5.1: L^1 and L^∞ error and order for “FD3RK3”, $T = 0.5$, $CFL = 0.6$, 1D linear equation with initial condition $u_0(x) = \sin^4(x)$, without limiters.

N	L^1 error	order	L^∞ error	order	$(u_h)_{min}$
20	2.21e-02	–	4.43e-02	–	-2.26E-02
40	3.49e-03	2.66	6.48e-03	2.77	-3.69E-03
80	4.54e-04	2.94	8.77e-04	2.89	-5.16E-04
160	5.76e-05	2.98	1.11e-04	2.98	-6.68E-05
320	7.22e-06	3.00	1.40e-05	3.00	-8.36E-06

Table 5.2: L^1 and L^∞ error and order for “FD3RK3”, $T = 0.5$, $CFL = 0.6$, 1D linear equation with initial condition $u_0(x) = \sin^4(x)$, with limiters.

N	L^1 error	order	L^∞ error	order	$(u_h)_{min}$
20	1.83e-02	–	4.43e-02	–	3.55E-14
40	3.24e-03	2.50	6.48e-03	2.77	1.23E-14
80	4.57e-04	2.82	8.77e-04	2.89	6.38E-23
160	5.75e-05	2.99	1.23e-04	2.83	1.72E-16
320	7.22e-06	2.99	1.71e-05	2.85	9.61E-22

Example 5.2. Consider the 1D nonlinear Burgers’ equation with periodic boundary conditions on $[0, 2\pi]$

$$u_t + \left(\frac{u^2}{2}\right)_x = 0, \quad u(x, 0) = u_0(x) \quad (5.2)$$

Table 5.3: L^1 and L^∞ error and order for “WENO5RK4”, $T = 0.5$, $CFL = 0.6$, 1D linear equation with initial condition $u_0(x) = \sin^4(x)$, without limiters.

N	L^1 error	order	L^∞ error	order	$(u_h)_{min}$
20	1.01e-02	–	1.90e-02	–	-2.58E-03
40	1.59e-03	2.66	4.27e-03	2.16	-5.93E-04
80	1.13e-04	3.82	6.00e-04	2.83	-5.64E-05
160	3.77e-06	4.90	2.74e-05	4.46	-1.20E-05
320	9.76e-08	5.27	7.59e-07	5.17	-2.03E-08

Table 5.4: L^1 and L^∞ error and order for “WENO5RK4”, $T = 0.5$, $CFL = 0.6$, 1D linear equation with initial condition $u_0(x) = \sin^4(x)$, with limiters.

N	L^1 error	order	L^∞ error	order	$(u_h)_{min}$
20	9.47e-03	–	1.90e-02	–	7.84E-15
40	1.49e-03	2.67	3.83e-03	2.31	1.16E-04
80	1.02e-04	3.86	5.42e-04	2.82	2.83E-05
160	3.26e-06	4.97	2.17e-05	4.64	2.18E-07
320	9.76e-08	5.06	7.59e-07	4.84	9.61E-15

and with the initial condition $u_0(x) = \sin^4(x)$. The exact solution is smooth up to $t = \frac{4\sqrt{3}}{9} \approx 0.7698$. The errors at $T = 0.5$ are reported in Tables 5.7-5.10. The numerical solutions are observed to enjoy the MPP property. The order of accuracy is maintained for both “FD3RK3” and “WENO5RK4”. After $t = \frac{4\sqrt{3}}{9}$, the solution develops a still shock. We show the solutions at $T = 1.2$ in Figure 5.1. For “FD3RK3” at mesh $N = 160$, without limiters, there are several large overshoots and undershoots. However with the MPP flux limiters, the overshoots and undershoots are completely under control with the minimum value $(u_h)_{min} = 3.90752E-22$ and the maximum value $(u_h)_{max} = 1.00000$. Without limiters, the minimum value for “WENO5RK4” is also negative, which is $(u_h)_{min} = -1.27153E-05$ at mesh $N = 160$, but with limiters, the minimum value is $(u_h)_{min} = 1.20706E-22$.

Example 5.3. Consider the 2D linear equation on $[-1, 1] \times [-1, 1]$

$$u_t + u_x + u_y = 0, \quad u(x, y, 0) = u_0(x, y) \quad (5.3)$$

with discontinuous initial condition

$$u_0(x, y) = \begin{cases} 1, & y \geq x; \\ -1, & y < x. \end{cases}$$

We show the cuts of numerical solutions for “FD3RK3” along $y + x = 0$ in Figure 5.2. With the MPP flux limiters, numerical solutions are observed to be non-oscillatory without

Table 5.5: L^1 and L^∞ error and order for “FD3RK3”, $T = 0.5$, $CFL = 1.0$, 1D linear equation with initial condition $u_0(x) = \sin^4(x)$, without limiters.

N	L^1 error	order	L^∞ error	order	$(u_h)_{min}$
20	2.54e-02	–	4.95e-02	–	-2.40E-02
40	4.42e-03	2.52	8.62e-03	2.52	-4.91E-03
80	5.98e-04	2.88	1.16e-03	2.90	-6.84E-04
160	7.70e-05	2.96	1.49e-04	2.96	-8.90E-05
320	9.72e-06	2.98	1.88e-05	2.99	-1.13E-05

Table 5.6: L^1 and L^∞ error and order for “FD3RK3”, $T = 0.5$, $CFL = 1.0$, 1D linear equation with initial condition $u_0(x) = \sin^4(x)$, with limiters.

N	L^1 error	order	L^∞ error	order	$(u_h)_{min}$
20	2.01e-02	–	4.94e-02	–	1.66E-23
40	4.11e-03	2.29	8.62e-03	2.52	0.00E-00
80	6.01e-04	2.77	1.16e-03	2.90	0.00E-00
160	7.69e-05	2.97	1.76e-04	2.71	1.19E-90
320	9.72e-06	2.98	2.27e-05	2.96	4.43E-158

overshoots and undershoots. For “WENO5RK4”, without limiters, the numerical solution is observed to be non-oscillatory. However, numerically it shows values under the minimum value -1 . For example, with mesh 100×100 , $(u_h)_{min} = -1.00133$ and $(u_h)_{max} = 1.00109$ from the scheme without limiters, but $(u_h)_{min} = -1.00000$ and $(u_h)_{max} = 1.00000$ from the scheme with limiters.

Example 5.4. Consider the 2D Burgers’ equation

$$u_t + \left(\frac{u^2}{2}\right)_x + \left(\frac{u^2}{2}\right)_y = 0, \quad u(x, y, 0) = u_0(x, y) \quad (5.4)$$

on $[0, 2\pi] \times [0, 2\pi]$ with periodic boundary conditions. The initial condition is $u_0(x, y) = \sin^4(x + y)$. The results are similar to the 1D case, see Tables 5.11-5.14. The cuts of the discontinuous solution along $x + y = 0$ are showed in Figure 5.3 at $T = 0.8$. With limiters, the numerical solution performs much better than the solution without limiters for “FD3RK3”. For the “WENO5RK4” scheme, the numerical solution is observed to be non-oscillatory. However, MPP property is violated from the scheme without limiters $(u_h)_{min} = -3.02538E - 05$. When the MPP limiter is applied, $(u_h)_{min} = 3.06377E - 15$.

Table 5.7: L^1 and L^∞ error and order for “FD3RK3”, $T = 0.5$, $CFL = 0.6$, 1D Burgers’ equation with initial condition $u_0(x) = \sin^4(x)$, without limiters.

N	L^1 error	order	L^∞ error	order	$(u_h)_{min}$	$(u_h)_{max}$
20	3.56e-02	–	1.47e-01	–	-2.39E-02	0.973
40	7.92e-03	2.17	5.05e-02	1.54	-3.95E-03	1.009
80	1.65e-03	2.26	1.85e-02	1.45	-4.71E-04	0.999
160	2.58e-04	2.68	4.12e-03	2.17	-6.02E-05	1.000
320	3.28e-05	2.97	6.75e-04	2.61	-7.56E-06	1.000
640	4.16e-06	2.98	8.70e-05	2.96	-9.46E-07	1.000

Table 5.8: L^1 and L^∞ error and order for “FD3RK3”, $T = 0.5$, $CFL = 0.6$, 1D Burgers’ equation with initial condition $u_0(x) = \sin^4(x)$, with limiters.

N	L^1 error	order	L^∞ error	order	$(u_h)_{min}$	$(u_h)_{max}$
20	3.32e-02	–	1.47e-01	–	1.05E-13	0.973
40	6.91e-03	2.26	5.04e-02	1.55	1.86E-15	1.000
80	1.65e-03	2.06	1.85e-02	1.45	9.85E-18	0.999
160	2.58e-04	2.68	4.12e-03	2.17	2.72E-22	1.000
320	3.28e-05	2.97	6.75e-04	2.61	1.13E-20	1.000
640	4.16e-06	2.98	8.70e-05	2.96	7.44E-21	1.000

5.2 Advection in incompressible flow

Example 5.5. Consider the rigid body rotation

$$u_t - (yu)_x + (xu)_y = 0, \quad x \in [-\pi, \pi], \quad y \in [-\pi, \pi]. \quad (5.5)$$

The initial condition includes a slotted disk, a cone as well as a smooth hump, see Figure 5.4. The cuts of the numerical solution for “FD3RK3” are displayed in the Figure 5.5. With limiters, the numerical solution is clearly within the range $[0, 1]$. For “WENO5RK4”, without limiter, the minimum value for the numerical solution is $(u_h)_{min} = -1.21853E-04$. With the limiter, the minimum value is strictly within the range $[0, 1]$ with $(u_h)_{min} = 6.22799E-15$. To save space, we omit the figure here.

Example 5.6. (Swirling deformation flow) Consider solving

$$u_t - \left(\cos^2\left(\frac{x}{2}\right) \sin(y)g(t)u\right)_x + \left(\sin(x) \cos^2\left(\frac{y}{2}\right)g(t)u\right)_y = 0, \quad x \in [-\pi, \pi], \quad y \in [-\pi, \pi] \quad (5.6)$$

with $g(t) = \cos(\pi t/T)\pi$. The initial condition is the same as Example 5.5. We also use “FD3RK3” and “WENO5RK4” to compute this example, for which similar results are observed. Solutions from “FD3RK3” with and without MPP limiters are displayed in Figure

Table 5.9: L^1 and L^∞ error and order for “WENO5RK4”, $T = 0.5$, $CFL = 0.6$, 1D Burgers’ equation with initial condition $u_0(x) = \sin^4(x)$, without limiters.

N	L^1 error	order	L^∞ error	order	$(u_h)_{min}$	$(u_h)_{max}$
20	2.74e-02	–	1.10e-01	–	-6.32E-04	0.934
40	4.03e-03	2.76	2.24e-02	2.30	-2.25E-04	0.990
80	6.81e-04	2.56	1.10e-02	1.03	-9.46E-05	0.998
160	6.79e-05	3.33	1.29e-03	3.10	-5.11E-06	1.000
320	2.97e-06	4.52	9.46e-05	3.77	-1.31E-08	1.000
640	1.07e-07	4.79	3.76e-06	4.65	-3.69E-10	1.000

Table 5.10: L^1 and L^∞ error and order for “WENO5RK4”, $T = 0.5$, $CFL = 0.6$, 1D Burgers’ equation with initial condition $u_0(x) = \sin^4(x)$, with limiters.

N	L^1 error	order	L^∞ error	order	$(u_h)_{min}$	$(u_h)_{max}$
20	2.72e-02	–	1.10e-01	–	9.73E-15	0.934
40	4.00e-03	2.77	2.25e-02	2.30	9.52E-15	0.990
80	6.74e-04	2.57	1.10e-02	1.03	8.92E-15	0.998
160	6.78e-05	3.31	1.29e-03	3.10	8.57E-22	1.000
320	2.97e-06	4.51	9.46e-05	3.77	9.73E-15	1.000
640	1.07e-07	4.79	3.76e-06	4.65	9.92E-15	1.000

5.6. For “WENO5RK4”, without the limiter, the minimum and maximum values for the numerical solution are $(u_h)_{min} = -1.74885E - 03$, $(u_h)_{max} = 1.01114$. With the limiter, $(u_h)_{min} = -2.57912E - 13$, $(u_h)_{max} = 1.00000$ within the range $[0, 1]$.

Example 5.7. Consider the incompressible Euler equations

$$\omega_t + (u\omega)_x + (v\omega)_y = 0, \quad (5.7)$$

$$\Delta\psi = \omega, \quad \langle u, v \rangle = \langle -\psi_y, \psi_x \rangle, \quad (5.8)$$

$$\omega(x, y, 0) = \omega_0(x, y), \quad \langle u, v \rangle \cdot \mathbf{n} = \text{given on } \partial\Omega \quad (5.9)$$

on the domain $[0, 2\pi] \times [0, 2\pi]$ with periodic boundary conditions. The initial condition $\omega_0(x, y) = -2 \sin(x) \sin(y)$. The exact solution stays stationary with $\omega(x, y, t) = -2 \sin(x) \sin(y)$. We tested the order of accuracy for “WENO5RK4” in Tables 5.15-5.16. We can see that the numerical solution with limiters can be within the range $[-2, 2]$ without affecting the order of accuracy. The numerical solution for “FD3RK3” is already within the range $[-2, 2]$ without limiters, the results with limiters are the same as those without limiters, so we do not list the results here.

Example 5.8. (The vortex patch problem) Consider the same problem as in Example 5.7,

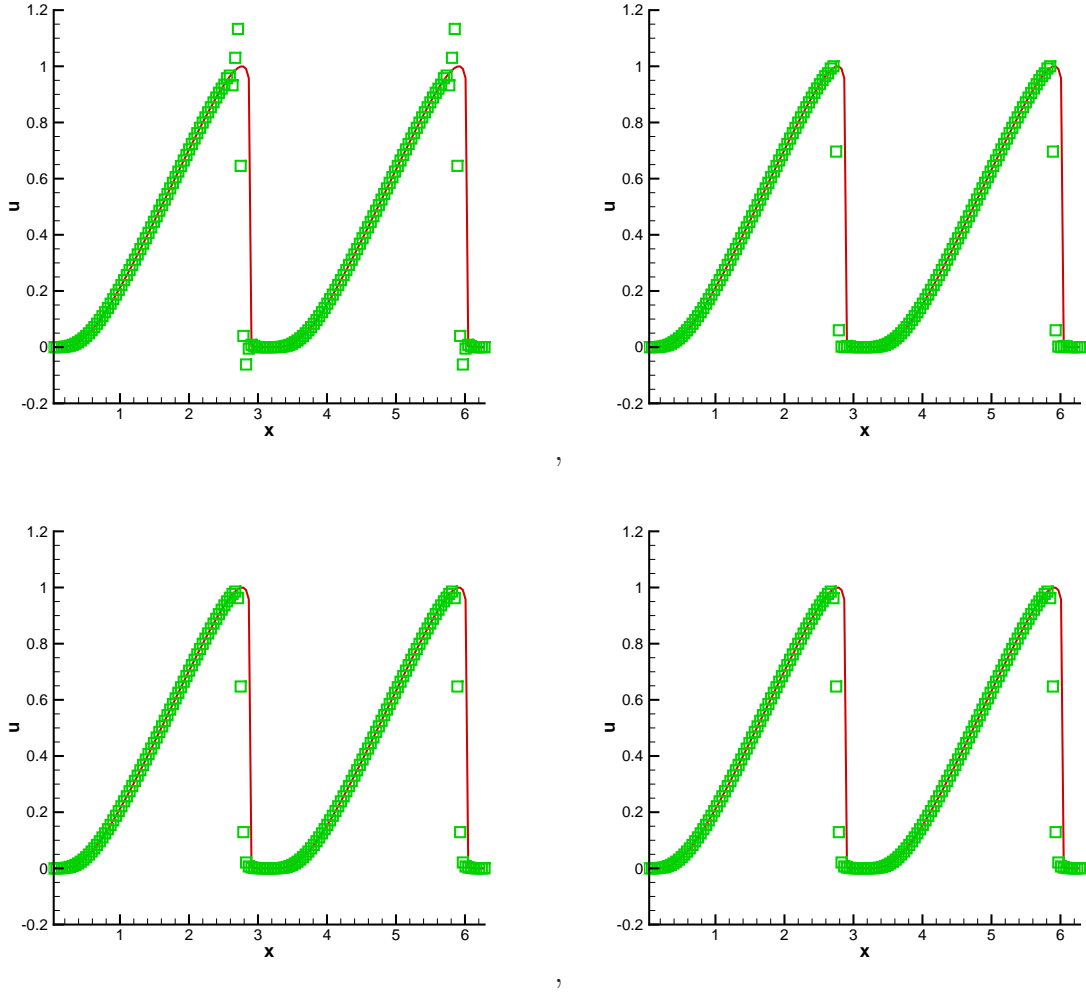


Figure 5.1: Numerical solutions for 1D Burgers' equation at $T = 1.2$. Mesh: $N = 160$. CFL=0.6. Left: without limiter; Right: with limiter. Top: FD3RK3; Bottom: WENO5RK4. Solid line: exact solution; Symbols: numerical solution.

but with the initial condition given by

$$\omega_0(x, y) = \begin{cases} -1, & \frac{\pi}{2} \leq x \leq \frac{3\pi}{2}, \frac{\pi}{4} \leq y \leq \frac{3\pi}{4}; \\ 1, & \frac{\pi}{2} \leq x \leq \frac{3\pi}{2}, \frac{5\pi}{4} \leq y \leq \frac{7\pi}{4}; \\ 0, & \text{otherwise.} \end{cases}$$

We show the contour plots of vorticity ω and the cut along the diagonal at $T = 5$ in Figure 5.7. The mesh size is 128×128 . For “FD3RK3” without the limiter, overshoots and undershoots are observed. However, the numerical solutions from the scheme with limiter are observed to be in the range of $[-1, 1]$. For “WENO5RK4”, we cannot observe any visible difference between the results without and with the limiter. The minimum and maximum values of the numerical solution without limiters are $(\omega_h)_{min} = -1.00051$ and $(\omega_h)_{max} = 1.00051$, and

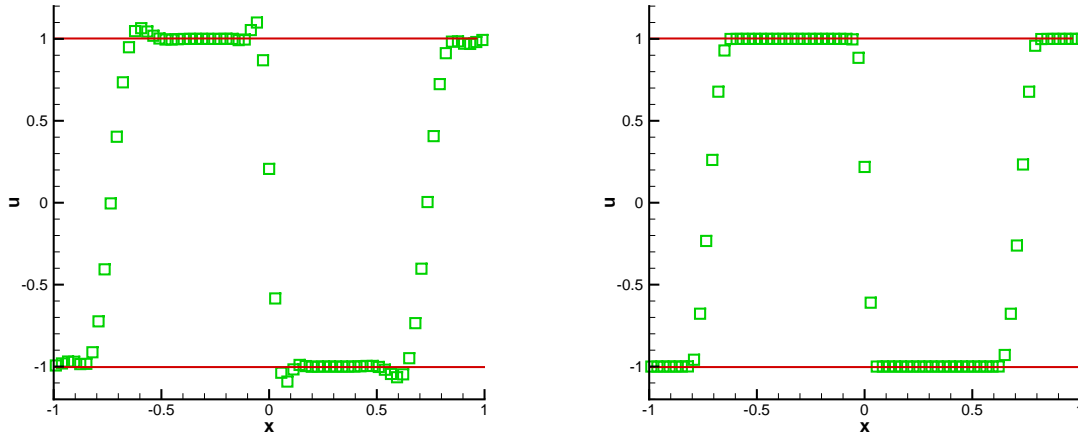


Figure 5.2: Numerical solutions for 2D linear problem with discontinuous initial condition for FD3RK3 at $T = 0.5$. Mesh: 100×100 . CFL=1. Left: without limiter; Right: with limiter. Cuts along $x + y = 0$. Solid line: referred maximal and minimal values ; Symbols: numerical solution.

with limiters are $(\omega_h)_{min} = -0.99998$ and $(\omega_h)_{max} = 0.99998$.

6 Conclusion

In this paper, we propose to apply a parametrized flux limiters only at the final stage of a multi-stage RK finite difference WENO schemes, to achieve the MPP property for solving scalar hyperbolic conservation laws. We use a formal local truncation error analysis to prove that, the proposed limiting approach maintains third order spatial and temporal accuracy if the high order flux is limited toward a first order local Lax-Friedrich flux or a Godunov flux under the linear stability condition of the original third order finite difference scheme. We also apply the MPP flux limiters to the conservative high order FD RK-WENO scheme solving the incompressible flow problems. Numerical experiments have demonstrated the efficiency and effectiveness of our new approach. Error analysis for arbitrarily high order schemes and extension to Euler systems will be explored in the future.

References

- [1] S. GOTTLIEB, D. KETCHESON, AND C.-W. SHU, *High order strong stability preserving time discretizations*, Journal of Scientific Computing, 38 (2009), pp. 251–289.

Table 5.11: L^1 and L^∞ error and order for “FD3RK3”, $T = 0.2$, $CFL = 1.0$, 2D Burgers’ equation with initial condition $u_0(x, y) = \sin^4(x + y)$, without limiters.

N	L^1 error	order	L^∞ error	order	$(u_h)_{min}$
20	2.66e-02	–	1.06e-01	–	-1.81E-02
40	5.08e-03	2.39	3.33e-02	1.67	-2.73E-03
80	8.46e-04	2.59	6.16e-03	2.43	-3.77E-04
160	1.09e-04	2.96	1.08e-03	2.52	-4.82E-05
320	1.37e-05	2.98	1.43e-04	2.92	-6.05E-06
640	1.70e-06	3.01	1.73e-05	3.04	-7.57E-07

Table 5.12: L^1 and L^∞ error and order for “FD3RK3”, $T = 0.2$, $CFL = 1.0$, 2D Burgers’ equation with initial condition $u_0(x, y) = \sin^4(x + y)$, with limiters.

N	L^1 error	order	L^∞ error	order	$(u_h)_{min}$
20	2.49e-02	–	1.05e-01	–	1.77E-15
40	4.92e-03	2.34	3.30e-02	1.68	1.22E-15
80	8.45e-04	2.54	6.16e-03	2.42	7.63E-16
160	1.09e-04	2.96	1.08e-03	2.52	6.91E-17
320	1.37e-05	2.98	1.43e-04	2.92	1.44E-19
640	1.70e-06	3.01	1.73e-05	3.04	1.73E-24

- [2] G.-S. JIANG AND C.-W. SHU, *Efficient implementation of weighted ENO schemes*, Journal of Computational Physics, 126 (1996), pp. 202–228.
- [3] D. LEVY, *A stable semi-discrete central scheme for the two-dimensional incompressible euler equations*, IMA journal of numerical analysis, 25 (2005), pp. 507–522.
- [4] S. OSHER, *Riemann solvers, the entropy condition, and difference approximations*, SIAM Journal on Numerical Analysis, 21 (1984), pp. 217–235.
- [5] C. SHEN, J.-M. QIU, AND A. CHRISTLIEB, *Adaptive Mesh Refinement Based on High order Finite Difference WENO Scheme for Multi-scale Simulations*, Journal of Computational Physics, 230 (2011), pp. 3780–3802.
- [6] C.-W. SHU, *Essentially non-oscillatory and weighted essentially non-oscillatory schemes for hyperbolic conservation laws*, Advanced numerical approximation of non-linear hyperbolic equations, (1998), pp. 325–432.
- [7] —, *High order weighted essentially non-oscillatory schemes for convection dominated problems*, SIAM Review, 51 (2009), pp. 82–126.

Table 5.13: L^1 and L^∞ error and order for “WENO5RK4”, $T = 0.2$, $CFL = 1.0$, 2D Burgers’ equation with initial condition $u_0(x, y) = \sin^4(x + y)$, without limiters.

N	L^1 error	order	L^∞ error	order	$(u_h)_{min}$
20	2.12e-02	–	8.86e-02	–	-4.61E-04
40	2.89e-03	2.88	1.65e-02	2.43	-1.51E-04
80	3.21e-04	3.17	2.78e-03	2.56	-7.91E-05
160	1.30e-05	4.63	2.31e-04	3.59	-3.86E-06
320	5.44e-07	4.57	9.37e-06	4.62	-1.04E-08
640	2.22e-08	4.61	3.20e-07	4.87	-2.92E-10

Table 5.14: L^1 and L^∞ error and order for “WENO5RK4”, $T = 0.2$, $CFL = 1.0$, 2D Burgers’ equation with initial condition $u_0(x, y) = \sin^4(x + y)$, with limiters.

N	L^1 error	order	L^∞ error	order	$(u_h)_{min}$
20	2.12e-02	–	8.86e-02	–	9.69E-15
40	2.88e-03	2.88	1.63e-02	2.44	9.50E-15
80	3.15e-04	3.19	2.78e-03	2.55	8.76E-15
160	1.27e-05	4.63	2.31e-04	3.59	9.41E-17
320	5.46e-07	4.55	9.37e-06	4.62	9.76E-15
640	2.22e-08	4.62	3.24e-07	4.85	9.93E-15

- [8] C.-W. SHU AND S. OSHER, *Efficient implementation of essentially non-oscillatory shock-capturing schemes*, Journal of Computational Physics, 77 (1988), pp. 439–471.
- [9] ———, *Efficient implementation of essentially non-oscillatory shock-capturing schemes, ii*, Journal of Computational Physics, 83 (1989), pp. 32–78.
- [10] P. K. SWEBY, *High resolution schemes using flux limiters for hyperbolic conservation laws*, SIAM journal on numerical analysis, 21 (1984), pp. 995–1011.
- [11] B. VAN LEER, *Towards the ultimate conservative difference scheme. ii. monotonicity and conservation combined in a second-order scheme*, Journal of computational physics, 14 (1974), pp. 361–370.
- [12] C. WANG, X. ZHANG, C.-W. SHU, AND J. NING, *Robust high order discontinuous galerkin schemes for two-dimensional gaseous detonations*, Journal of Computational Physics, 231 (2012), pp. 653–665.
- [13] Y. XING, X. ZHANG, AND C.-W. SHU, *Positivity-preserving high order well-balanced discontinuous galerkin methods for the shallow water equations*, Advances in Water Resources, 33 (2010), pp. 1476–1493.

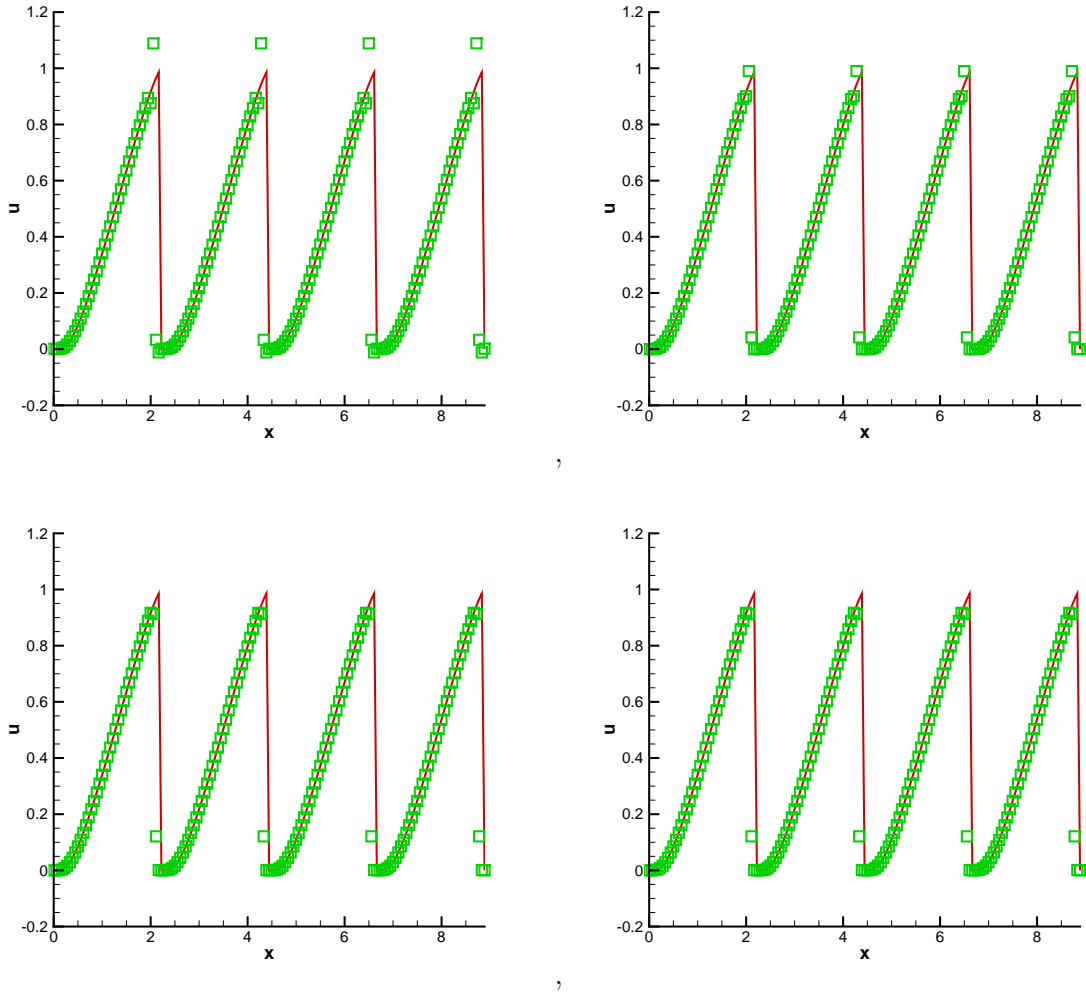


Figure 5.3: Numerical solutions for 2D Burgers' equation at $T = 0.8$. Mesh: 160×160 . CFL=1. Left: without limiter; Right: with limiter. Cuts along $y + x = 0$. Top: FD3RK3; Bottom: WENO5RK4. Solid line: exact solution; Symbols: numerical solution.

- [14] Z. XU, *Parametrized maximum principle preserving flux limiters for high order scheme solving hyperbolic conservation laws: one-dimensional scalar problem*, Mathematics of Computation, (accepted).
- [15] Z. XU AND C. LIANG, *Parametrized Maximum-principle-preserving flux limiters for high order schemes solving multi-dimensional scalar hyperbolic conservation laws*, Journal of Scientific Computing, (submitted).
- [16] X. ZHANG AND C.-W. SHU, *On maximum-principle-satisfying high order schemes for scalar conservation laws*, Journal of Computational Physics, 229 (2010), pp. 3091–3120.

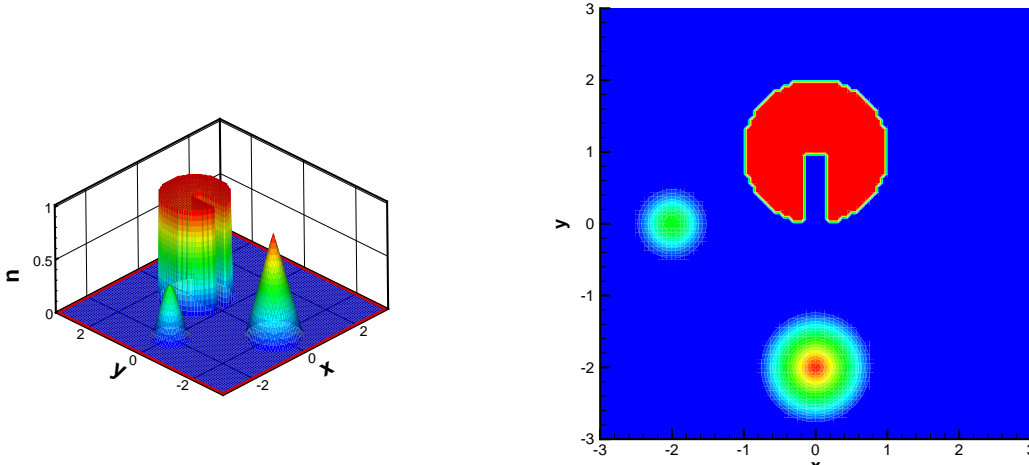


Figure 5.4: Plots of the initial profile for equation (5.5). Mesh: 100×100 .

[17] —, *On positivity-preserving high order discontinuous galerkin schemes for compressible euler equations on rectangular meshes*, *Journal of Computational Physics*, 229 (2010), pp. 8918–8934.

[18] —, *Maximum-principle-satisfying and positivity-preserving high-order schemes for conservation laws: survey and new developments*, *Proceedings of the Royal Society A: Mathematical, Physical and Engineering Science*, 467 (2011), pp. 2752–2776.

[19] —, *Positivity-preserving high order finite difference weno schemes for compressible euler equations*, *Journal of Computational Physics*, 231 (2012), pp. 2245–2258.

[20] X. ZHANG, Y. XIA, AND C.-W. SHU, *Maximum-principle-satisfying and positivity-preserving high order discontinuous galerkin schemes for conservation laws on triangular meshes*, *Journal of Scientific Computing*, 50 (2012), pp. 29–62.

Table 5.15: L^1 and L^∞ error and order for “WENO5RK4”, $T = 0.1$, $CFL = 1.0$, incompressible Euler equations with initial condition $\omega_0(x, y) = -2\sin(x)\sin(y)$, without limiters.

N	L^1 error	order	L^∞ error	order	$(u_h)_{min} - u_{min}$	$u_{max} - (u_h)_{max}$
40	7.85E-05	–	3.76E-04	–	-1.69E-06	-1.69E-06
80	4.71E-06	4.06	3.60E-05	3.39	-6.77E-08	-6.77E-08
160	1.86E-07	4.66	1.60E-06	4.49	-1.57E-09	-1.57E-09
320	6.94E-09	4.75	7.58E-08	4.40	-2.60E-11	-2.60E-11
640	1.32E-10	5.71	1.42E-09	5.74	2.68E-13	2.68E-13

Table 5.16: L^1 and L^∞ error and order for “WENO5RK4”, $T = 0.1$, $CFL = 1.0$, incompressible Euler equations with initial condition $\omega_0(x, y) = -2\sin(x)\sin(y)$, with limiters.

N	L^1 error	order	L^∞ error	order	$(u_h)_{min} - u_{min}$	$u_{max} - (u_h)_{max}$
40	7.85E-05	–	3.76E-04	–	9.99E-14	9.99E-14
80	4.71E-06	4.06	3.60E-05	3.39	9.99E-14	9.99E-14
160	1.86E-07	4.66	1.60E-06	4.49	9.99E-14	9.99E-14
320	6.94E-09	4.75	7.58E-08	4.40	9.99E-14	9.99E-14
640	1.32E-10	5.71	1.42E-09	5.74	2.76E-13	2.77E-13

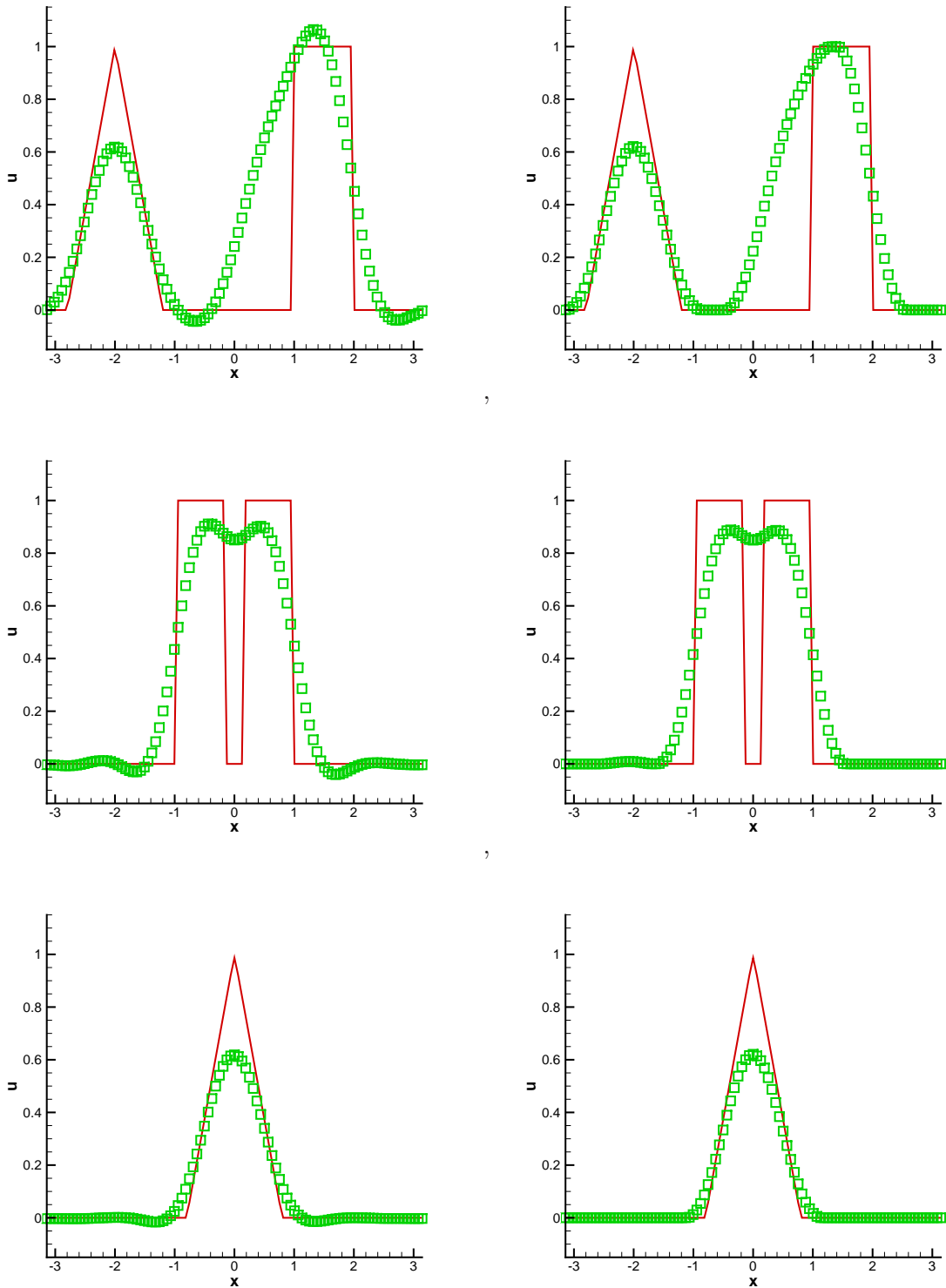


Figure 5.5: Plots of slides of numerical solutions for equation (5.5) with FD3RK3 at $T = 12\pi$. Mesh: 100×100 . CFL=1. Left: without limiter; Right: with limiter. Cuts along $x = 0$, $y = 0.8$ and $y = -2$ from top to bottom, respectively. Solid line: exact solution; Symbols: numerical solution.

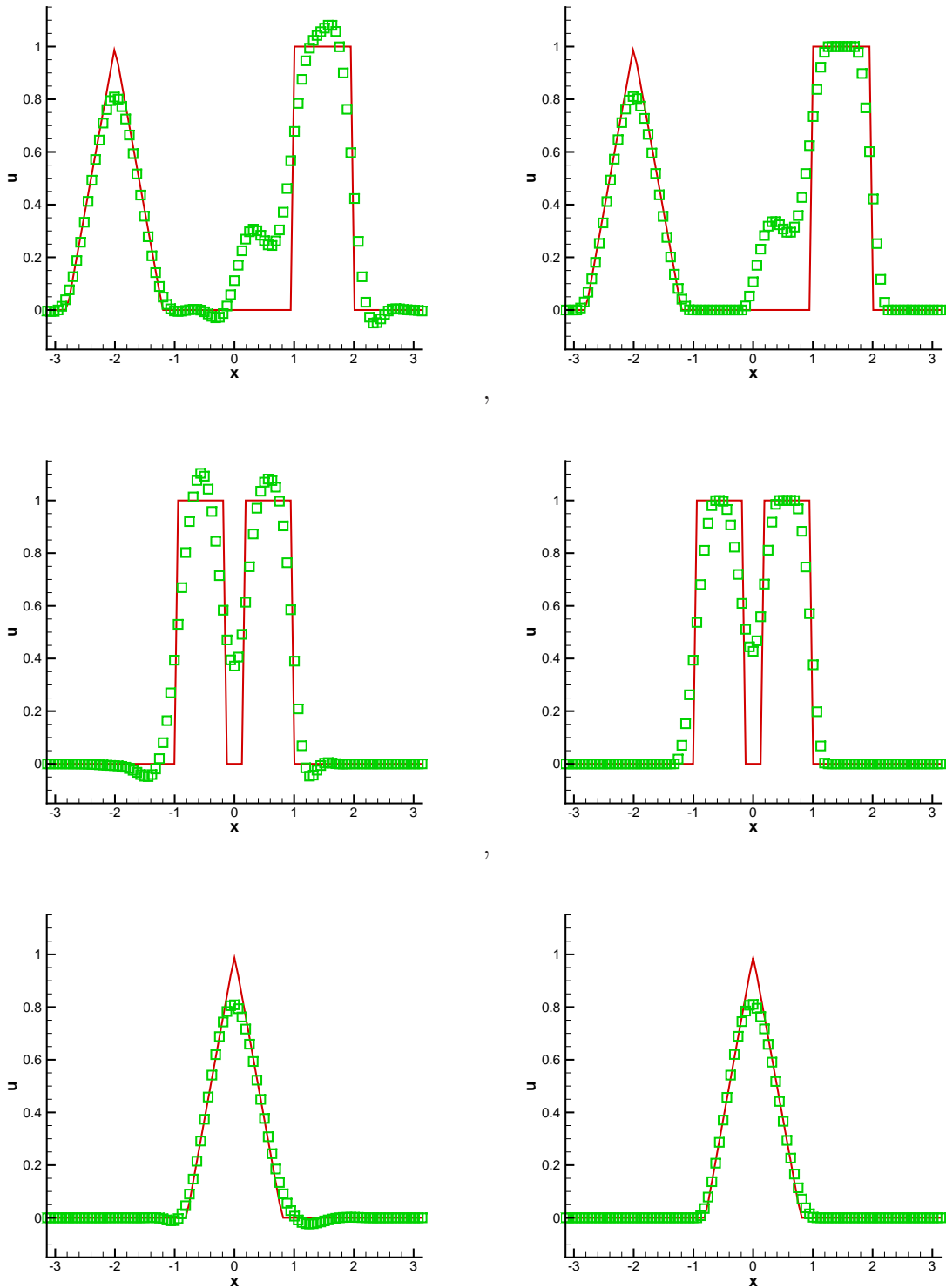


Figure 5.6: Plots of slides of numerical solutions for equation (5.6) with FD3RK3 at $T = 1.5$. Mesh: 100×100 . CFL=1. Left: without limiter; Right: with limiter. Cuts along $x = 0$, $y = 0.8$ and $y = -2$ from top to bottom, respectively. Solid line: exact solution; Symbols: numerical solution.

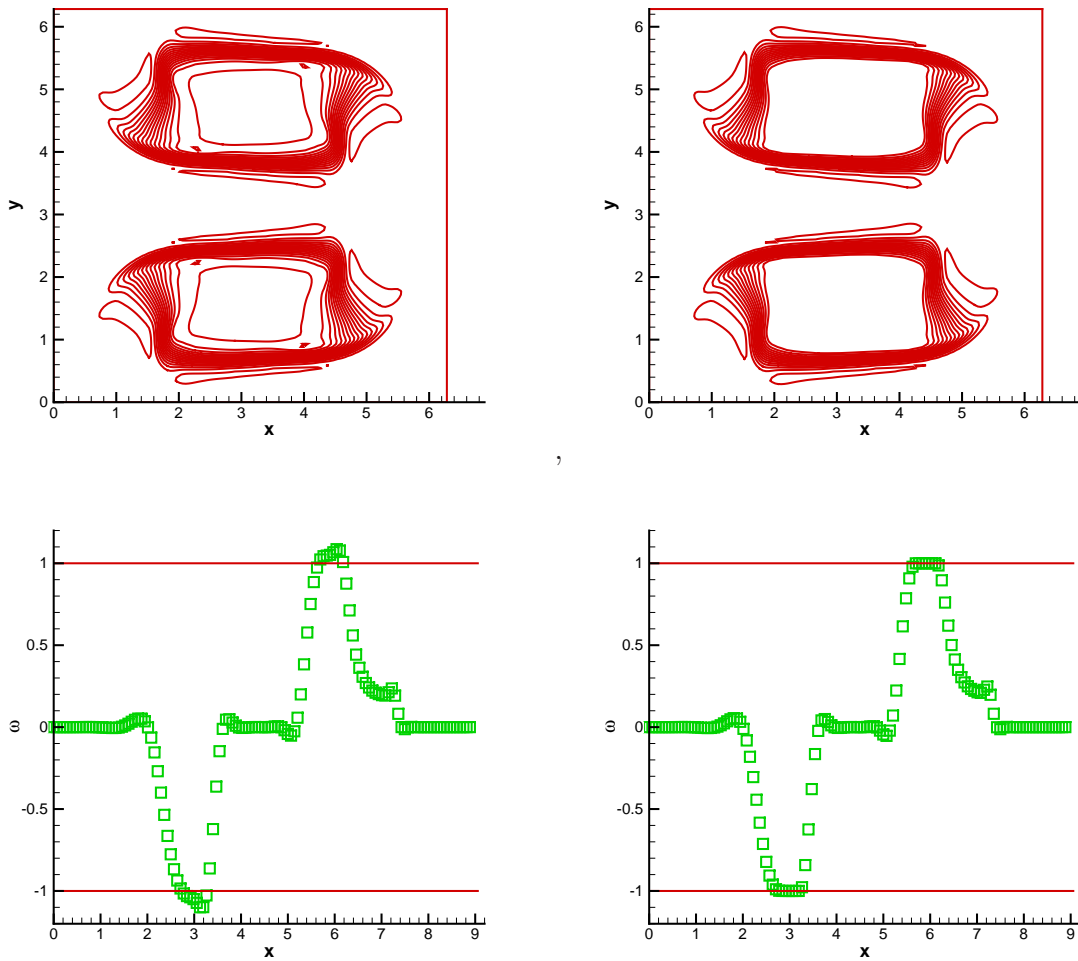


Figure 5.7: Plots of numerical solutions for Example 5.8 with FD3RK3 at $T = 5$. Mesh: 128×128 . CFL=1. Left: without limiter; Right: with limiter. Top: 30 equally spaced contours from -1.1 to 1.1; bottom: cut along the diagonal. Solid line: referred maximal and minimal values ; Symbols: numerical solution.